Supplementary Information

A small-sized benzothiazole-indolium fluorescent probe: the study of interaction specificity targeting c-MYC promoter G-quadruplex structures and live cell imaging

Bo-Xin Zheng [a], Meng-Ting She [a], Wei Long [a], Yong-Yu Xu [a], Yi-Han Zhang [a], Xuan-He Huang [a], Wenjie Liu [c], Jin-Qiang Hou [c], Wing-Leung Wong [b,d,*] and Yu-Jing Lu [a,*]

[a] School of Biomedical and Pharmaceutical Sciences, Guangdong University of Technology, Guangzhou 510006, P. R. China.

[b] State Key Laboratory of Chemical Biology and Drug Discovery, Department of Applied Biology Chemical Technology, The Hong Kong Polytechnic University, Hung Hom, Kowloon, Hong Kong, China.

[c] Department of Chemistry, Lakehead University and Thunder Bay Regional Health Research Institute, 980 Oliver Road, Thunder Bay, On, P7B 6V4, Canada.

[d] School of Biotechnology and Health Sciences, Wuyi University, Jiangmen, 529020, P.R. China.

* Corresponding author

E-mail (W.-L. Wong): wing.leung.wong@polyu.edu.hk; wleungwong@outlook.com

E-mail (Y.-J. Lu): luyj@gdut.edu.cn.

List of contents

added subsequently, the concentration ratio is 10/1. (B) CD spectra of pu27 (5 μM) interacted with the probe without K^+ ion and with 60 mM KCl in 10 mM Tris-HCl buffer at pH 7.4.

Figure S6. CD spectra of c-MYC G4-DNA (5 μM) interacted with different concentration of **BZT-Indolium** (1 to 3 equivalents) in 10 mM Tris-HCl buffer with 60 mM KCl at pH 7.4: (A) pu18; (B) pu22; (C) pu24; and (D) pu27.

Figure S7. (A) Linear relationship of probe **BZT-Indolium** in the detection of pu18; (B) Linear relationship of probe **BZT-Indolium** in the detection of pu22; (C) Linear relationship of probe **BZT-Indolium** in the detection of pu24; (D) Linear relationship of probe **BZT-Indolium** in the detection of pu27. The concentration of **BZT-Indolium** was 0.5 μM in Tris−HCl buffer (10 mM, pH 7.4) containing 60 mM KCl.

Figure S8. UV-vis titration spectra of **BZT-Indolium** (10 μM) with different concentration of c-MYC G4-DNA in a Tris-HCl buffer (10 mM, pH = 7.4) containing 60 mM KCl: (A) pu18; (B) pu22; (C) pu24; and (D) pu27.

Figure S9. (A) The linear fitting of the absorption intensity by the fluorescence emission spectral integral area of **BZT-Indolium** in pu18; (B) The linear fitting of the absorption intensity by the fluorescence emission spectral integral area of **BZT-Indolium** in pu22; (C) The linear fitting of the absorption intensity by the fluorescence emission spectral integral area of **BZT-Indolium** in pu24; (D) The linear fitting of the absorption intensity by the fluorescence emission spectral integral area of **BZT-Indolium** in pu27. The concentration of **BZT-Indolium** was 0.5 μM in Tris−HCl buffer (10 mM, pH 7.4) containing 60 mM KCl.

Figure S10. (A) Gel electrophoresis (20 % acrylamide in 1 × TBE) of da21, ds26, 4at, telo21, pu18, pu22, pu24, pu27 at a concentration of 5.0 μM and was stained with **BZT-Indolium** (5.0 μM) for 15 min; (B) Gel electrophoresis (20 % acrylamide in 1 × TBE) of da21, ds26, 4at, telo21, pu18, pu22, pu24, pu27 at a concentration of 5.0 μM and was stained with **SYBR Gold** (5.0 μM) for 15 min.

Figure S11. The curve of fluorescence intensity with time (1 h) after the combination of probe **BZT-Indolium** (0.5 μM) with c-MYC promoter G4-DNA (pu18, pu22, pu24, pu27) (1.0 μM). The excitation wavelength λ_{ex} = 434 nm, the emission wavelength λ_{em} = 477 nm.

Figure S12. Fluorescence decay traces of **BZT-Indolium** (0.5 μM, λ_{ex} = 320 nm, λ_{em} = 477 nm) in the absence and in the presence of different DNA substrates including ds26, telo21, pu18, pu22, pu24 and pu27 in 10 mM Tris-HCl buffer at pH 7.4 containing 60 mM KCl.

Figure S13. The evaluation the G4-structure stabilization ability of **BZT-Indolium** in 10 mM Tris-HCl buffer at pH 7.4 containing 60 mM KCl: (A) Normalized CD signal of pu18 during melting process; (B) Normalized CD signal of pu22 during melting process; (C) Normalized CD signal of pu24 during melting process; (D) Normalized CD signal of pu27 during melting process. The G-quadruplex was characterized by the positive peak at 262 nm.

Figure S14. The evaluation the stabilization ability of **BZT-Indolium** in 10 mM Tris-HCl buffer at pH 7.4 containing 60 mM KCl: (A) Normalized CD signal of double stranded DNA (ds26) during melting process, the double stranded DNA was characterized by the negative peak at 242 nm; (B) Normalized CD signal of Telomere G4-DNA (telo21) during melting process, the G-quadruplex was characterized by the positive

peak at 290 nm; (C) Normalized CD signal of Telomere G4-DNA (Htg24) during melting process, the G-quadruplex was characterized by the positive peak at 290 nm.

Figure S15. Expression rate of c-MYC mRNA at different concentrations of **BZT-Indolium**.

Figure S16. Fluorescence binding assays of **BZT-Indolium** with pu22 mutants in Tris–HCl buffer containing 60 mM KCl. Fluorescence signal change = F_{pu22} mutant-F_{pu22} wild type.

Figure S17. The molecular docking study of **BZT-Indolium** in complex with pu22 G-quadruplex.

Figure S18. (A) Fluorescence images of live MCF-7 cells stained with 5.0 μM **BZT-Indolium** for 15 min; (B) Fluorescence images of live MCF-7 cells stained with 5.0 μM **BZT-Indolium** for 15 min and RNase treated for 2 h; (C) Fluorescence images of live MCF-7 cells stained with 5 μM **BZT-Indolium** for 15 min and DNase treated for 2 h.

Figure S19. Fluorescence images of live non-cancer cells 16HBE stained with 5.0 μM **BZT-Indolium** for 15 min.

Figure S20. Intracellular competition experiments in live U87 cells and images were taken after incubated for 15 min: (A) 5 μM probe; (B) 5 μM probe and then 5 μM BRACO19; (C) 5 μM probe and then 10 μM BRACO19.

Figure S21. Fluorescence response of **BZT-Indolium** (0.5 μM) added to pu27 G4-DNA and BRACO19 was added subsequently. The concentration ratio between **BZT-Indolium** and BRACO19 is 1: 1 and 1: 2.

Figure S22. (A) Cells survival viability of U87 cells; (B) Cells survival viability of HeLa cells; (C) Cells survival viability of MCF7 cells; (D) Cells survival viability of 16HBE cells; (E) Cells survival viability of HK2 cells. The concentration gradients of **BZT-Indolium** were 0, 0.3125, 0.625, 1.25, 5, 10 and 20 μM.

Figure S23. Fluorescence titration spectra of **BZT-Indolium** with different nucleic acids: RNA; single-stranded DNA: da21, dt21; duplex DNA: 4a4t, hairpin, ds12, ds26, 4at; Telomere G4-DNA: human12, telo21, Htg22, Htg24, 4telo21, oxy12; Promoter G4-DNA: RET, ckit1, ckit2, VEGF, Kras, Hras, bcl2, pu18, pu22, pu24 and pu27 in a Tris-HCl buffer (10 mM, pH 7.4) containing 60 mM KCl. Fluorescence signal was measured at 25 °C.

Figure S24. Fluorescence titrations, presented as a relative increase of the integral fluorescence (F/F_0) of different nucleic acids: RNA; single-stranded DNA: da21, dt21; duplex DNA: 4a4t, hairpin, ds12, ds26, 4at; Telomere G4-DNA: human12, telo21, Htg22, Htg24, 4telo21, oxy12; Promoter G4-DNA: RET, ckit1, ckit2, VEGF, Kras, Hras, bcl2, pu18, pu22, pu24 and pu27 with **BZT-Indolium** (0.5 μM) in 10 mM Tris-HCl buffer (pH 7.4, containing 60 mM KCl).

Figure S25. (A) The UV absorption spectrum obtained by adding five continuous concentrations (0.4 μM, 0.8 μM, 1.2 μM, 1.6 μM ,2.0 μM) of **BZT-Indolium** to a fixed concentration of 1 μM pu18; (B) The UV absorption spectrum obtained by adding five continuous concentrations (0.4 μM, 0.8 μM, 1.2 μM, 1.6 μM ,2.0 μM) of **BZT-Indolium** to a fixed concentration of 1 μM pu22; (C) The UV absorption spectrum obtained by adding five continuous concentrations (0.4 μM, 0.8 μM, 1.2 μM, 1.6 μM, 2.0 μM) of **BZT-Indolium** to a fixed concentration of 1 μM pu24; (D) The UV absorption spectrum obtained by adding five

continuous concentrations (0.4 μM, 0.8 μM, 1.2 μM, 1.6 μM, 2.0 μM) of **BZT-Indolium** to a fixed concentration of 1 μM pu27.

Figure S26. (A) Fluorescence spectrum obtained by adding five continuous concentrations of **BZT-Indolium** (0.4 μM, 0.8 μM, 1.2 μM, 1.6 μM, 2.0 μM) to a fixed concentration of 1 μM pu18; (B) Fluorescence spectrum obtained by adding five continuous concentrations of **BZT-Indolium** (0.4 μM, 0.8 μM, 1.2 μM, 1.6 μM, 2.0 μM) to a fixed concentration of 1 μM pu22; (C) Fluorescence spectrum obtained by adding five continuous concentrations of **BZT-Indolium** (0.4 μM, 0.8 μM, 1.2 μM, 1.6 μM, 2.0 μM) to a fixed concentration of 1 μM pu24; (D) Fluorescence spectrum obtained by adding five continuous concentrations (0.4 μM, 0.8 μM, 1.2 μM, 1.6 μM, 2.0 μM) of **BZT-Indolium** to a fixed concentration of 1 μM pu27.

Figure S27. UV-vis titration spectra of **BZT-Indolium** (10 μM) with selected nucleic acids in a Tris-HCl buffer (10 mM, pH = 7.4) with 60 mM KCl at 25 °C: (A) RNA. (B) dt21. (C) ds26. (D) telo21 G4-DNA.

Figure S28. Fluorescence titration spectra of **BZT-Indolium** with different concentrations of pu22 mutants. The concentration of **BZT-Indolium** was 0.5 μM in Tris−HCl buffer (10 mM, pH 7.4) containing 60 mM KCl.

Figure S29. CD spectra of 5 μM pu22/A3C, pu18/A3G, pu22/A3T, pu22/T7A, pu22/T7C, pu22/T7G, pu22/T11A, pu22/T11C, pu22/T11G, pu22/A12C, pu22/A12G, pu22/A12T, pu22/T16A, pu22/T16C, pu22/T16G binding to **BZT-Indolium** in 10 mM Tris-HCl buffer at pH 7.4 with 60 mM KCl.

Figure S30. ^{1}H NMR (DMSO-d_6), HRMS of intermediate **A**.

Figure S31. ^{1}H NMR (DMSO-d_6), HRMS of intermediate **B**.

Figure S32. ^{1}H NMR (DMSO-d_6), ^{13}C NMR (DMSO-d_6), HRMS of **BZT-Indolium**.

Section A: Experimental

1. Materials

All the reagents and chemicals are AR grade and need no further purification. All the oligonucleotides were synthesized and purified by Thermo Fisher Scientific and their sequences were listed in **Table S1**. Besides, ^{1}H and ^{13}C NMR spectra were recorded at 400 MHz and 100 MHz in DMSO-d_6 with a Bruker BioSpin GmbH spectrometer. High resolution mass spectra (HRMS) were obtained by Agilent 1260-6230 TOF. The cell lines used in this study including U87 cells (human glioma cells, ATCC® HTB-14™), HeLa cells (human cervical cancer cells, ATCC® CRM-CCL-2™), MCF7 cells (human breast cancer cells, ATCC® HTB-22™), 16HBE cells (Immortalized human bronchial epithelial cells, ATCC® CRL-4051™), and HK2 (human renal tubular epithelial cells, ATCC® CRL-2190™) were purchased from ATCC.

2. The synthesis and characterization of BZT-Indolium:

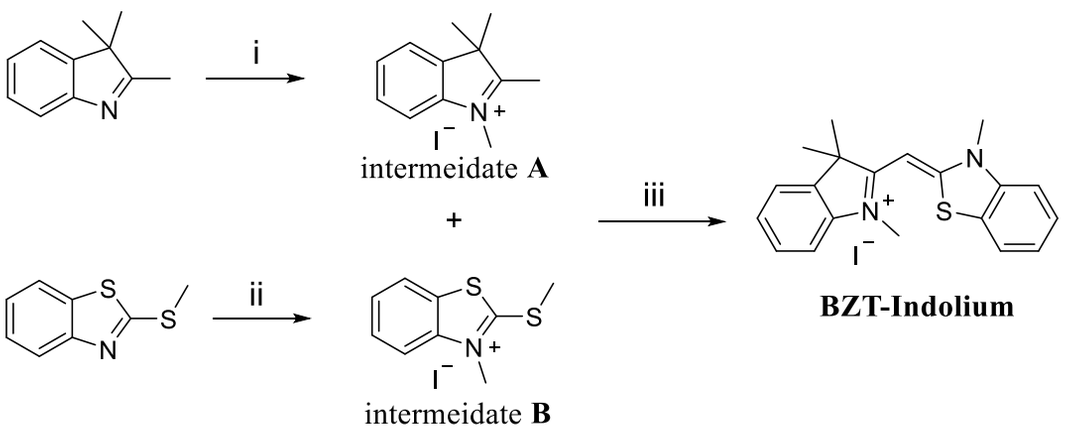

Scheme S1. Synthesis route to **BZT-Indolium** and its molecular structures. Reagents and conditions: (i) iodomethane, acetonitrile, 80 °C, 8 h; (ii) iodomethane, acetonitrile, 80 °C, 8 h; (iii) acetonitrile, triethylamine, 70 °C, 8 h.

2.1 Synthesis of intermediate A: 1,2,3,3-tetramethyl-3H-indol-1-ium

2,3,3-trimethyl-3H-indole (2.0 mmol) and iodomethane (3.0 mmol) was added to a clean round bottom flask and then add 8.0 ml of acetonitrile to dissolve them. The mixture was refluxed at 80 ℃ for 8 h. After the reaction was confirmed by TLC, 15.0 ml ethyl acetate was added to precipitate the solid, and the intermediate **A** was obtained by recrystallization of ethanol. The compounds were characterized with ^{1}H NMR. Pink solid, yield 85.7 %. ^{1}H NMR (400 MHz, DMSO) δ 7.92 (dd, J = 5.7, 3.0 Hz, 1H), 7.85 – 7.81 (m, 1H), 7.63 (dd, J = 6.3, 2.7 Hz, 2H), 3.98 (s, 3H), 2.77 (s, 3H), 1.54 (s, 6H). HRMS m/z: calcd for $C_{12}H_{16}^{+}$, $[M\text{-}I]^{+}$ = 174.1279, found 174.1279.

2.2 Synthesis of intermediate B: 3-methyl-2-(methylthio)benzo[d]thiazol-3-ium

2-(methylthio)benzo[d]thiazole (2.0 mmol) and iodomethane (3.0 mmol) was added to a clean round bottom flask and then add 8.0 ml of acetonitrile to dissolve them. The mixture was refluxed at 80 ℃ for 8 h. After the reaction was confirmed by TLC, 15.0 ml ethyl acetate was added to precipitate the solid, and

the intermediate **B** was obtained by recrystallization of ethanol. The compounds were characterized with ^{1}H NMR. White solid, yield 83.4 %. ^{1}H NMR (400 MHz, DMSO) δ 8.41 (dd, *J* = 8.1, 0.6 Hz, 1H), 8.21 (d, *J* = 8.4 Hz, 1H), 7.85 (dd, *J* = 8.5, 7.4, 1.2 Hz, 1H), 7.76 – 7.71 (m, 1H), 4.12 (s, 3H), 3.14 (s, 3H). HRMS m/z: calcd for $C_9H_{10}NS_2^+$, $[M-I]^+$ = 196.0245, found 196.0245.

2.3 Synthesis of BZT-Indolium: (Z)-1,3,3-trimethyl-2-((3-methylbenzo[d]thiazol-2(3H)-ylidene)methyl)-3H-indol-1-ium

The intermediates **A** (1.5 mmol) and **B** (1.5 mmol) was added to a clean round bottom flask and then add 6.0 ml of acetonitrile to dissolve them. In addition, triethylamine (0.5 mmol) was added as catalyst. The mixture was refluxed at 70 ℃ for 8 h. After the reaction was confirmed by TLC, 10.0 ml ethyl acetate was added to precipitate the solid, and the end products **BZT-Indolium** were obtained by recrystallization of ethanol. The compounds were characterized with ^{1}H, ^{13}C NMR, and HRMS. Orange solid, yield 76.6 %. ^{1}H NMR: (400 MHz, DMSO) δ 8.17 (d, *J* = 7.4 Hz, 1H), 7.97 (d, *J* = 8.4 Hz, 1H), 7.71 (m, 1H), 7.57 (m, 2H), 7.41 (m, 2H), 7.26 (t, *J* = 7.3, 1H), 6.08 (s, 1H), 4.05 (s, 3H), 3.60 (s, 3H), 1.69 (s, 6H). ^{13}C NMR (101 MHz, DMSO): δ 174.82, 165.11, 144.01, 141.14, 139.93, 128.92, 126.44, 125.22, 123.70, 122.84, 115.24, 111.57, 82.89, 49.80, 35.52, 25.32. HRMS m/z: calcd for $C_{20}H_{21}N_2S^+$, $[M-I]^+$ = 321.1416, found 321.1416.

3. Methods

3.1 UV-Vis and fluorescence analysis

In this study, the UV-Vis spectrum was obtained by using Lambda 25 Spectrophotometer (Perkin Elmer). The fluorescence spectrum was recorded on the LS-45 fluorescence spectrometer (Perkin Elmer). The slit width of the colorimetric dish is 1 mm and optical diameter is 10 mm.

The calculation of fluorescence quantum yields was based on the equation: $\Phi_x = \Phi_{ST} (Grad_x / Grad_{ST}) (\eta^2_x / \eta^2_{ST})$.[1] In the equation, the subscript ST represents standard, the subscript X represents test, Φ represents fluorescence quantum yields, Grad represents gradient from the plot of integrated fluorescence intensity versus absorbance, and η represents refractive index of the solvent. In the present study, the standard used was fluorescein (1 % NaOH ethanol, Φ = 0.95).[2]

3.2 Fluorescence lifetime study

Fluorescence lifetime decays were recorded using HORIBA Fluorolog. The method is time-correlated single-photon counting (TCSPC). The experiments were performed using 0.5 μM concentration of the **BZT-Indolium** in 10 mM Tris-HCl buffer at pH 7.4 containing 60 mM KCl, λ_{ex} = 320 nm, λ_{em} = 477 nm. The slit is 29 nm.

3.3 The limit of detection (LOD)

The limit of detection (LOD) of the compounds were obtained by fluorescence titration and estimated based on the calculation formula: LOD = K (S_b/m). In the equation, S_b is the standard deviation of the blank multiple measurements (n = 20), and m is the slope of the calibration curve, which represents the sensitivity of this method. In addition, according to the International Union of Pure and Applied Chemistry (IUPAC), K value is generally taken to be 3.

3.4 Circular dichroism (CD) and melting point test

The CD spectra were performed on a Chirascan spectrophotometer (Applied Photophysics). During the experiment, a quartz cuvette with a length of 1 mm was used to record the spectrum in a wavelength range of 220 to 340 nm with a 1 nm bandwidth, a 1 nm step and 0.5 s per point. The melting point test was set at a fixed wavelength, while gradually increasing the temperature from 25 to 95 °C, 1 nm step size, and 5 s per point. The experiments were performed using 8 μM **BZT-Indolium** and 4 μM DNA in 10 mM Tris-HCl buffer at pH 7.4 containing 60 mM KCl.

3.5 NMR titration

Experiments were performed on 600 MHz Bruker spectrometers at 25 °C. The G4 samples for ^{1}D NMR were prepared in a phosphate buffer (25 mM KH_2PO_4, 70 mM KCl, 10 % D_2O, pH 7.4) with pu22 G4-DNA. The final concentration of G4-DNA was 300 μM and was titrated with compound **BZT-Indolium**. The final concentration of **BZT-Indolium** was 900 μM.

3.6 Native PAGE experiment conditions

The gel electrophoresis was based on 30 % (29:1) polyacrylamide gels with a size of 160 x 140 x 0.75 mm. The oligonucleotides used in the experiment included various single-, duplex- and quadruplex-forming oligonucleotides, with a fixed concentration of 5 μM, and they were run in 1 x TBE buffer (80 mM Tris-borate, 2 mM EDTA, pH 8.3). The experimental parameters were as follows: temperature = 0 °C, voltage = 110 V, time = 4 h. Finally, the removed gel was stained with compound **BZT-Indolium** (5 μM) in 1 x TBE for 20 min. Meanwhile, a commercial SYBR Gold (5 μM) was used to stain another gel as a control.[3]

3.7 Fluorescence microscopy imaging study and cell staining

Cancer cells human glioma cells (U87), human breast cancer cells (MCF7) and non-cancer cells human bronchial epithelial cells (16HBE) were cultured in confocal dishes for 24 h. After the removal of medium, the confocal dishes were washed with pre-cooled PBS for three times. After washing, the cells were fixed by pre-cooled 99 % methanol (-4 °C) for 1 min. Then, the sample was washed with pre-cooled PBS for 3 times. **BZT-Indolium** (5 μM) was added and then stained for 15 min. Finally, the confocal dishes were washed with pre-cooled PBS for six times and then it was observed under confocal microscope. The excitation wavelengths was 434 nm for **BZT-Indolium**. The digital images were then recorded on confocal laser scanning microscopy (ZEISS LSM 800 with Airscan).

3.8 DNase and RNase digestion tests

On the basis of fluorescence microscopy imaging study, 1 mL DNase (Sigma, 50 μg/mL) and RNase (GE, 50 μg/mL) were added to the confocal dishes respectively and then the sample was cultured at 37 °C for 2 h under 5 % CO_2. After that, the solution was removed from the confocal dishes and the sample was washed with pre-cooled PBS for 6 times. Finally, the digital images were recorded on confocal laser scanning microscopy (ZEISS LSM 800 with Airscan).

3.9 Confocal imaging of co-localization

Cancer cells human glioma cells (U87) were cultured in confocal dishes for 24 h. After the removal of medium, the confocal dishes were washed with pre-cooled PBS for three times. After washing, the cells were fixed by pre-cooled 99 % methanol (-4 °C) for 1 min. Then, the sample was washed with pre-cooled PBS for 3 times. **BZT-Indolium** (5.0 μM) was added and then stained for 15 min. After that, the sample was washed with pre-cooled PBS for 3 times, and TMPyP4 (5.0 μM) was added and then stained for 15 min. Finally, the confocal dishes were washed with pre-cooled PBS for six times and then it was observed under confocal microscope. The excitation wavelength of **BZT-Indolium** is set to 434 nm and that of TMPyP4 is set to 647 nm. The digital images were then recorded on confocal laser scanning microscopy (ZEISS LSM 800 with Airscan).

3.10 Cell competitive test

Cancer cells human glioma cells (U87) were cultured in confocal dishes for 24 h. After the removal of medium, the confocal dishes were washed with pre-cooled PBS for three times. After washing, the cells were fixed by pre-cooled 99 % methanol (-4 °C) for 1 min. Then, the sample was washed with pre-cooled PBS for 3 times. **BZT-Indolium** (5.0 μM) was added and then stained for 15 min. After that, the sample was washed with pre-cooled PBS for 3 times, and BRACO19 (5.0 μM and 10.0 μM) was added for 15 min. Finally, the confocal dishes were washed with pre-cooled PBS for six times and then it was observed under confocal microscope. The excitation wavelength of **BZT-Indolium** is set to 434 nm. The digital images were then recorded on confocal laser scanning microscopy (ZEISS LSM 800 with Airscan).

3.11 PCR stop assay

Polymerase stop assay was performed using a modified protocol previous reported.[4] In short, the PCR stop assay was conducted by introducing different concentrations of compound (0–15 μM) into 25 μl solution containing 1X PCR buffer, 2 μM of each oligomer, 0.16 mM dNTP and 2.5 U Taq polymerase (Invitrogen, USA). Reaction mixtures were incubated in a thermocycler under the following cycling conditions: 94 °C for 5 min, 30 cycles of 94 °C for 30 s, 56 °C for 30 s and 72 °C for 30 s. Amplified products were resolved on 20 % polyacrylamide gel and stained with SYBR Gold (Invitrogen, USA).

3.12 RT-PCR

HeLa cells were incubated in 6-well plates with different concentrations of **BZT-Indolium** (0, 2, 5, 10, 20 μM) for 48 hours, then the medium was removed and washed three times with precooled PBS. HeLa cells were dissolved with TRIzol, and the total RNA was extracted according to the manufacturer's instructions. Finally, the extracted RNA was dissolved in distilled deionized water containing 0.1% diethyl pyrocarbonate (DEPC), and the final volume was 50 μL. Each reaction mixture (20 μL) contained 2 × One Step SYBR Green Mix 10 μL, One Step SYBR Green Enzyme Mix 1 μL, 50 × ROX Reference Dye 1 0.4 μL, Gene Specific Primer Forward (10 μM) 0.4 μL, Gene Specific Primer Reverse (10 μM) 0.4 μL, 1 μg of total RNA and RNase-free ddH2O to 20 μL. The reaction mixtures were incubated in a thermocycler under the following cycling conditions: denature at 94 °C for 3 min, followed by 30 cycles at 94 °C for 45 s, 60 °C for 30 s and 72 °C for 45 s, and elongation 72 °C for 10 min. Amplified products were resolved on

20 % polyacrylamide gel and stained with SYBR Gold (Invitrogen, USA). The primers used in the real-time RT-PCR were as follows: c-MYCA, 5′-TGGTGCTCCATGAGGAGACA-3′; c-MYCS, 5′-GTGGCACCTCTTGAGGACCT-3′. GAPDH is used as an internal control for normalization, the internal control GAPDH is amplified by the forward primer 5′-GGGAAACTGTGGCGTGAT-3′ and the reverse primer 5′-GAGTGGGTGTCGCTGTTGA-3′. A comparative Ct (ΔΔCT) method was used to compare the mRNA expression levels of genes of interest.

3.13 MTT assay

Both cancer cells U87 cells, HeLa cells and MCF7 cells and non-cancer cells, 16HBE cells and HK2 cells, were used in the MTT experiments. The cells were cultured on 96-well plates with a density of 5000 cells per well approximately. The culture medium were DMEM (U87), DMEM (HeLa), DMEM (MCF7), DMEM (16HBE) and HK2 (F12) and the culture condition was set at 37 °C and 0.5 % CO_2. After cultured for 24 h, the 96-well plate was washed three times with pre-cooled PBS and then U87 cells, 16HBE cells and HK2 cells were treated with **BZT-Indolium** solutions at different concentrations (0, 0.3125, 0.625, 1.25, 2.5, 5, 10, and 20 μM) for 48 h, respectively. After culture, the medium was decanted and 5 mg/mL of MTT solution, 200 μL per well, was added to the sample and then incubated for 4 h in dark. Then, the MTT solution was decanted and DMSO (100 μL per well) was added to ensure the deck adhering to 96-well plate complete dissolution. These treated 96-well plates were measured for absorbance with an enzyme label and the absorption wavelength was 577 nm. Finally, the cell survival rate and the half maximal inhibitory concentration (IC_{50}) of compound **BZT-Indolium** on the cells were calculated from the obtained absorbance values.

3.14 Molecular docking study

The solution structure of human c-MYC promoter G4-DNA was used to perform molecular docking studies (PDB ID: 6o2l).[5] The 3D structure of BZT-Indolium ligand were generated using DS viewer 3.5. Molecular docking was performed using AUTODOCK vina program.[6] The dimensions of the grid box were set large enough to encompass the whole G-quadruplex structure. All other parameters were left as default.

Section B: Supporting Tables and Figures

Table S1. Sequences of oligonucleotides used in the present study.

Abbreviation	Source/Sequence (5′→3′)	Structure/origin
RNA	16S- and 23S-Ribosomal from *E. coli*	Duplex
da21	AAAAAAAAAAAAAAAAAAAAA	Single-stranded
dt21	TTTTTTTTTTTTTTTTTTTT	Single-stranded
4a4t	AAAATTTT	Duplex
hairpin	CGCGCGCGTTTTCGCGCGCG	Duplex
ds12	GCGCAATTGCGC	Duplex
ds26	CAATCGGATCGAATTCGATCCGATTG	Duplex
4at	GCGCAATTGCGC	Duplex
human12	TTAGGGTTAGGG	Telomere G-quadruplex
telo21	GGGTTAGGGTTAGGGTTAGGG	Telomere G-quadruplex
Htg22	AGGGTTAGGGTTAGGGTTAGGG	Telomere G-quadruplex
Htg24	TTGGGTTAGGGTTAGGGTTAGGGA	Telomere G-quadruplex
4telo21	GGGTTAGGGTTAGGGTTAGGGTTAGGGTTAG	Telomere G-quadruplex
oxy12	GGGGTTTTGGGG	Telomere G-quadruplex
RET	GGGGCGGGGCGGGGCGGGGG	Promoter G-quadruplex
ckit1	AGGGAGGGCGCTGGGAGGAGGG	Promoter G-quadruplex
ckit2	GGGCGGGCGCGAGGGAGGGG	Promoter G-quadruplex
VEGF	GGGGCGGGCCGGGGGCGGGG	Promoter G-quadruplex
Kras	GGGCGGTGTGGGAAGAGGGAAGAGGGG	Promoter G-quadruplex
Hras	TCGGGTTGCGGGCGCAGGGCACGGGCG	Promoter G-quadruplex
bcl2	GGGCGCGGGAGGAAGGGGGCGGG	Promoter G-quadruplex
pu18	AGGGTGGGGAGGGTGGGG	Promoter G-quadruplex
pu22	TGAGGGTGGGTAGGGTGGGTAA	Promoter G-quadruplex
pu24	TGAGGGTGGGGAGGGTGGGGAAGG	Promoter G-quadruplex
pu27	TGGGGAGGGTGGGGAGGGTGGGGAAGG	Promoter G-quadruplex

Table S2. F/F_0 and binding constants for **BZT-Indolium** with different oligonucleotide determined from the fitted curves (λ_{ex} = 434 nm, λ_{em} = 477 nm).

Oligonucleotides	Binding signal, F/F_0 [a]	Binding constants [b] K_{eq} ($\times 10^5$ M^{-1})
RNA	2.8	n.d.
da21	6.6	2.74±0.18
dt21	8.3	3.48±0.14
4a4t	1.3	n.d.
hairpin	1.7	n.d.
ds12	1.7	n.d.
ds26	3.0	n.d.
4at	4.1	1.95±0.21
human12	10.0	5.06±0.67
telo21	14.7	7.13±1.04
Htg22	14.8	7.42±0.46
Htg24	16.5	7.79±0.38
4telo21	16.9	8.25±0.92
oxy12	19.0	9.63±0.28
RET	26.6	11.18±1.17
ckit1	30.5	14.54±1.33
ckit2	35.9	16.98±0.85
VEGF	36.8	17.28±1.04
Kras	38.8	18.47±1.12
Hras	48.6	24.25±1.98
bcl2	54.7	27.81±1.06
pu18	90.3	40.53±1.57
pu22	85.8	37.74±1.73
pu24	75.3	34.07±1.65
pu27	73.1	33.92±1.29

[a] The concentrations of **BZT-Indolium** and oligonucleotides are 0.5 μM and 9.0 μM.

[b] Equilibrium binding constant of **BZT-Indolium** with oligonucleotides at 25 °C; n.d. denoted as not determined because the ligand-DNA binding signal is too weak for estimation.

Table S3. The spectroscopic data of **BZT-Indolium** with c-MYC G-quadruplex DNA.[a]

	Absorbance (λ_{max}, nm)	λ_{em} (nm)	Stokes shift	Φ_f [b]	Lifetime (ns)	K_{eq} ($\times 10^5$ M^{-1})	LOD [c] (nM)	Lr [e] (μM)	R^2
pu18	434	477, 502	43, 68	0.28±0.022	4.49	40.53±1.57	1.63	0.142-2.84	0.9816
pu22	434	477, 502	43, 68	0.24±0.015	4.07	37.74±1.73	1.27	0.142-2.272	0.9873
pu24	434	477, 502	43, 68	0.23±0.013	4.12	34.07±1.65	2.53	0.284-2.84	0.9803
pu27	434	477, 502	43, 68	0.19±0.025	4.20	33.92±1.29	1.65	0.284-2.272	0.9774

[a] Experiments were performed in a 10 mM Tris-HCl buffer at pH 7.4 containing 60 mM KCl; λ_{ex} = 434 nm.
[b] Relative fluorescence quantum yield of **BZT-Indolium** upon addition of c-MYC promoter G4-DNA at 9.0 μM. The standard of the relative fluorescence quantum yield is fluorescein (Φ_f = 0.95, methanol with 1% NaOH);
[c] Limit of detection for c-MYC promoter G4-DNA;
[d] Equilibrium binding constant between the compound and c-MYC promoter G4-DNA at 25 °C;
[e] Linear detection range of c-MYC promoter G4-DNA.

Table S4. Sequences of pu22 oligonucleotides used in the present study.

Abbreviation	Sequence (5′→3′)	Structure/origin
pu22	TGAGGGTGGGTAGGGTGGGTAA	G-quadruplex
pu22/A3T	TG**T**GGGTGGGTAGGGTGGGTAA	G-quadruplex
pu22/A3C	TG**C**GGGTGGGTAGGGTGGGTAA	G-quadruplex
pu22/A3G	TG**G**GGGTGGGTAGGGTGGGTAA	G-quadruplex
pu22/T7A	TGAGGG**A**GGGTAGGGTGGGTAA	G-quadruplex
pu22/ T7C	TGAGGG**C**GGGTAGGGTGGGTAA	G-quadruplex
pu22/ T7G	TGAGGG**G**GGGTAGGGTGGGTAA	G-quadruplex
pu22/ T11A	TGAGGGTGGG**A**AGGGTGGGTAA	G-quadruplex
pu22/ T11C	TGAGGGTGGG**C**AGGGTGGGTAA	G-quadruplex
pu22/ T11G	TGAGGGTGGG**G**AGGGTGGGTAA	G-quadruplex
pu22/ A12C	TGAGGGTGGGT**C**GGGTGGGTAA	G-quadruplex
pu22/ A12G	TGAGGGTGGGT**G**GGGTGGGTAA	G-quadruplex

pu22/ A12T	TGAGGGTGGGT**T**GGGTGGGTAA	G-quadruplex
pu22/ T16A	TGAGGGTGGGTAGGG**A**GGGTAA	G-quadruplex
pu22/ T16C	TGAGGGTGGGTAGGG**C**GGGTAA	G-quadruplex
pu22/ T16G	TGAGGGTGGGTAGGG**G**GGGTAA	G-quadruplex
An illustration model of pu22 G4-DNA	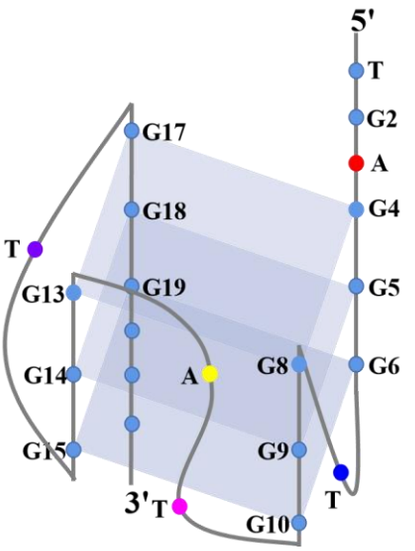	

Table S5. IC_{50} of **BZT-Indolium** against the cell lines.[a]

Cell lines	IC_{50} (μM)
U87	20.18±0.76
HeLa	8.68±1.15
MCF7	11.41±1.34
16HBE	25.15±0.68
HK2	33.68±0.97

[a] Data are presented in mean±SD of three independence experiments and each was performed in triplicate.

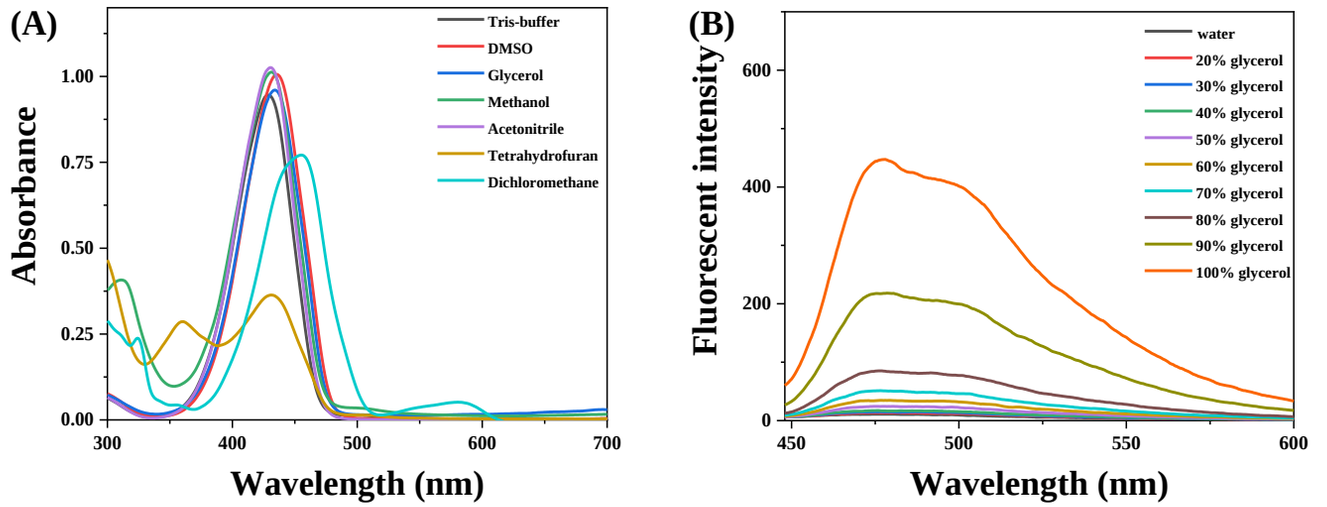

Figure S1. (A) Absorption spectra of 20 μM of **BZT-Indolium** in different solvents, including Tris-buffer, DMSO, glycerol, methanol, acetonitrile, tetrahydrofuran and dichloromethane; (B) Fluorescent intensity of **BZT-Indolium** in different glycerol ratios. The concentration of the compound was 0.5 μM.

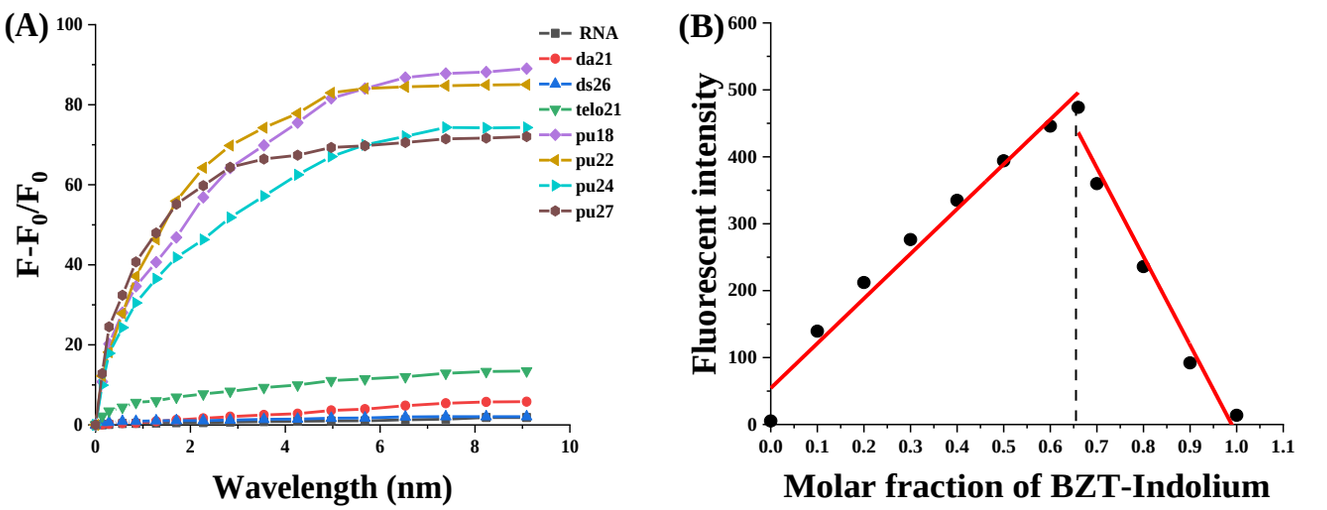

Figure S2. (A) Fluorescence titration of the probe **BZT-Indolium** with different concentrations of RNA, da21, ds26, telo21, pu18, pu22, pu24 and pu27. Fluorescence signal was measured at 25 °C, and the concentration of **BZT-Indolium** was 0.5 μM in Tris−HCl buffer (10 mM, pH 7.4) containing 60 mM KCl. F_0 represents the fluorescence intensity of **BZT-Indolium** itself, and F represents the maximum fluorescence intensity of **BZT-Indolium** after binding with nucleic acids. (B) Job plot analysis of binding stoichiometry of **BZT-Indolium** and pu27.

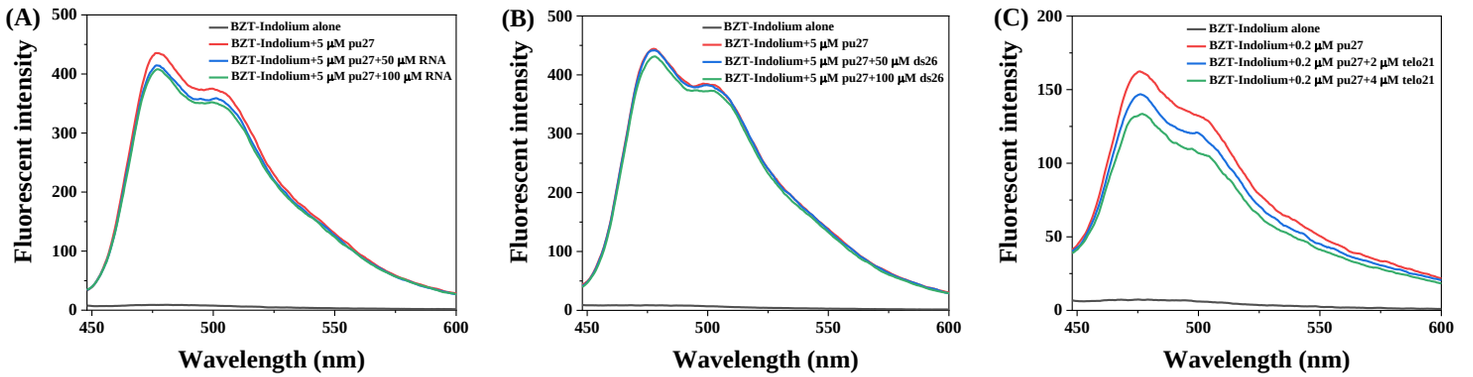

Figure S3. *In vitro* competition study of **BZT-Indolium** between pu27 G4-DNA and other nucleic acids: (A) pu27 at 5 μM and RNA was added at the concentrations 50 μM and 100 μM; (B) pu27 at 5 μM and double-stranded DNA (ds26) was added at the concentrations 50 μM and 100 μM; (C) pu27 at 0.2 μM and telo21 G4-DNA was added at the concentrations 2 μM and 4 μM. The concentration of **BZT-Indolium** was 0.5 μM in Tris−HCl buffer (10 mM, pH 7.4) containing 60 mM KCl.

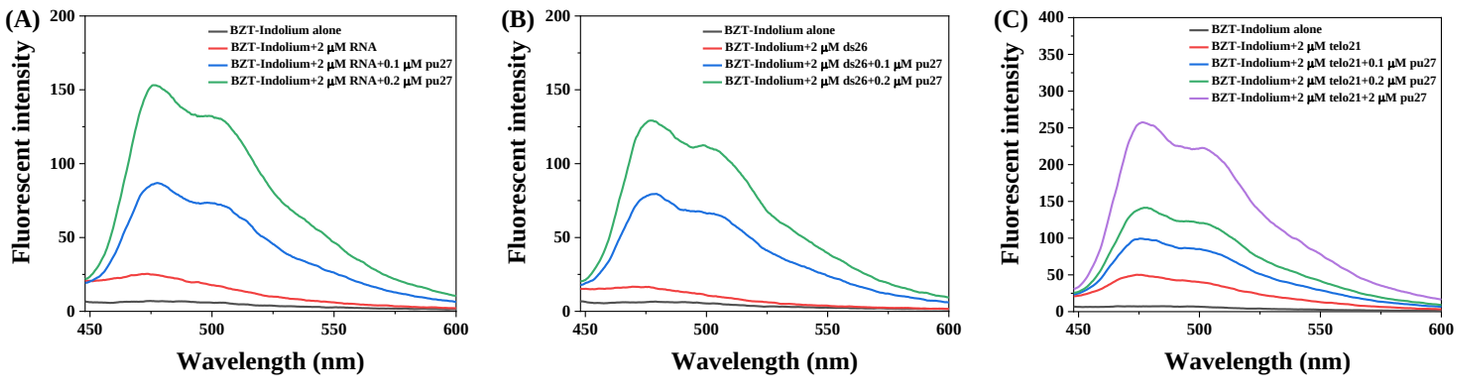

Figure S4. *In vitro* competition study of **BZT-Indolium** between pu27 G4-DNA and other nucleic acids: (A) 0.1 and 0.2 μM pu27 G4-DNA was added subsequently to compete with RNA at 2 μM; (B) 0.1 and 0.2 μM pu27 G4-DNA was added subsequently to compete with double-strand DNA (ds26) at 2 μM; (C) 0.1, 0.2 and 2 μM pu27 G4-DNA was added subsequently to compete with telo21 G4-DNA at 2 μM. The concentration of **BZT-Indolium** was 0.5 μM in Tris−HCl buffer (10 mM, pH 7.4) containing 60 mM KCl.

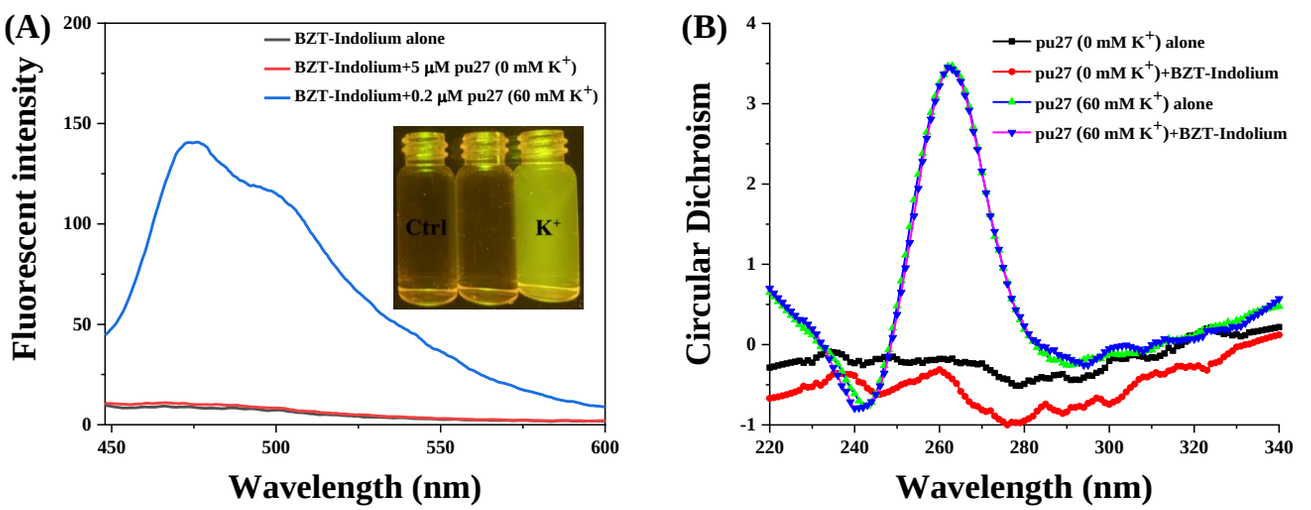

Figure S5. Study of conformational effects of **BZT-Indolium** on the G4-structure: (A) Fluorescence response of **BZT-Indolium** to K^+ free pu27 G4-DNA and pu27 G4-DNA which contains 60 mM K^+ was added subsequently, the concentration ratio is 10/1. (B) CD spectra of pu27 (5 μM) interacted with the probe without K^+ ion and with 60 mM KCl in 10 mM Tris-HCl buffer at pH 7.4.

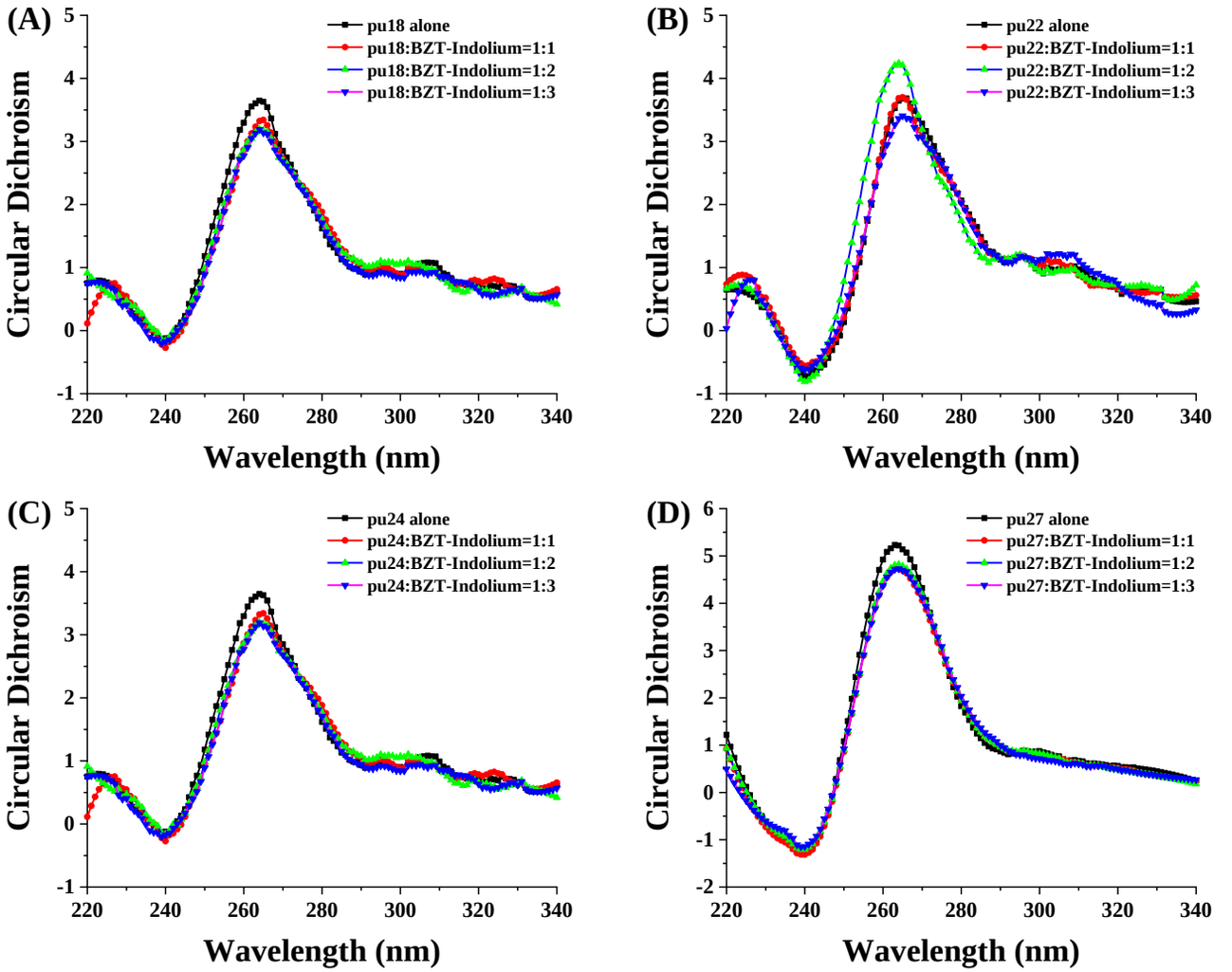

Figure S6. CD spectra of c-MYC G4-DNA (5 μM) interacted with different concentration of **BZT-Indolium** (1 to 3 equivalents) in 10 mM Tris-HCl buffer with 60 mM KCl at pH 7.4: (A) pu18; (B) pu22; (C) pu24; and (D) pu27.

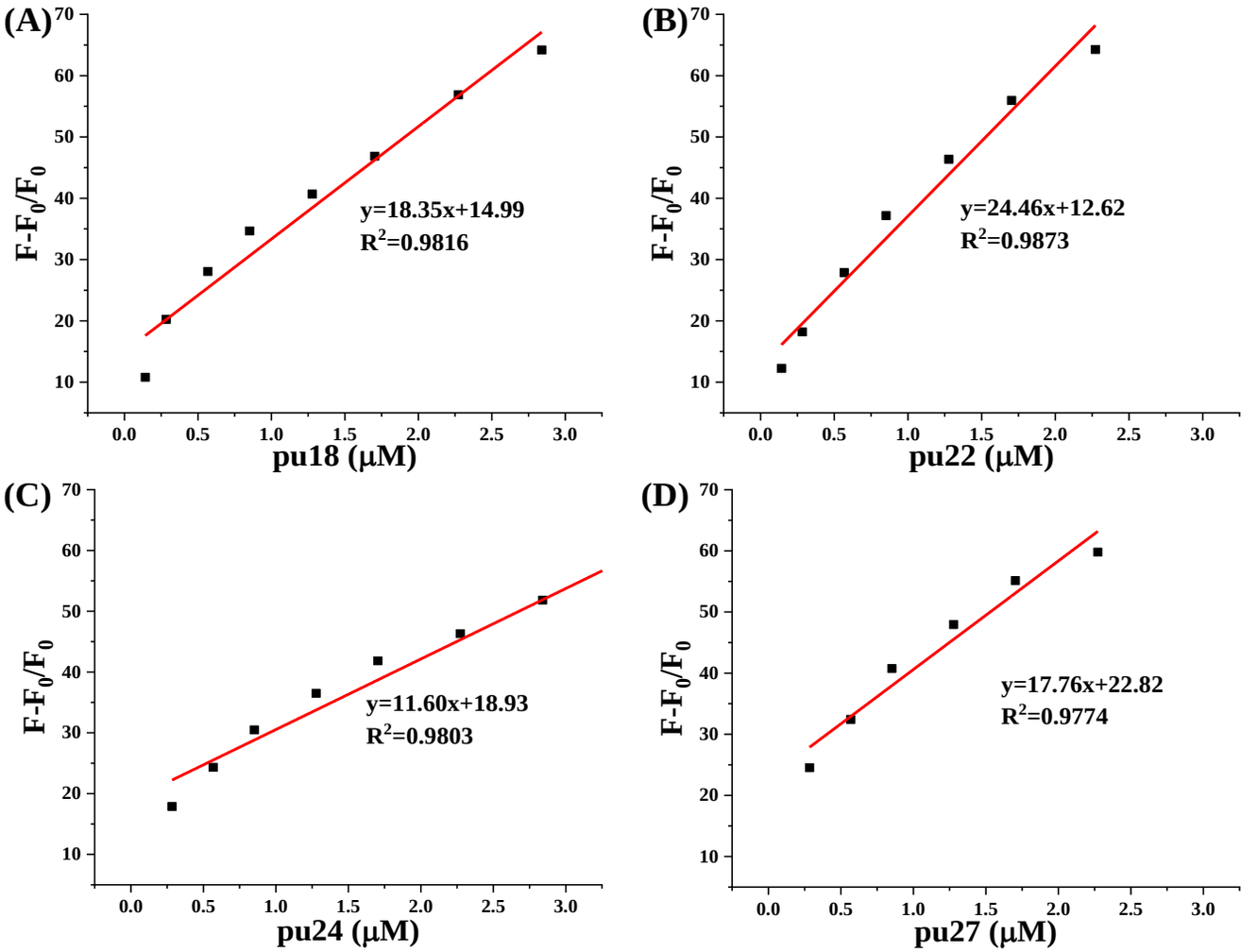

Figure S7. (A) Linear relationship of probe **BZT-Indolium** in the detection of pu18; (B) Linear relationship of probe **BZT-Indolium** in the detection of pu22; (C) Linear relationship of probe **BZT-Indolium** in the detection of pu24; (D) Linear relationship of probe **BZT-Indolium** in the detection of pu27. The concentration of **BZT-Indolium** was 0.5 μM in Tris−HCl buffer (10 mM, pH 7.4) containing 60 mM KCl.

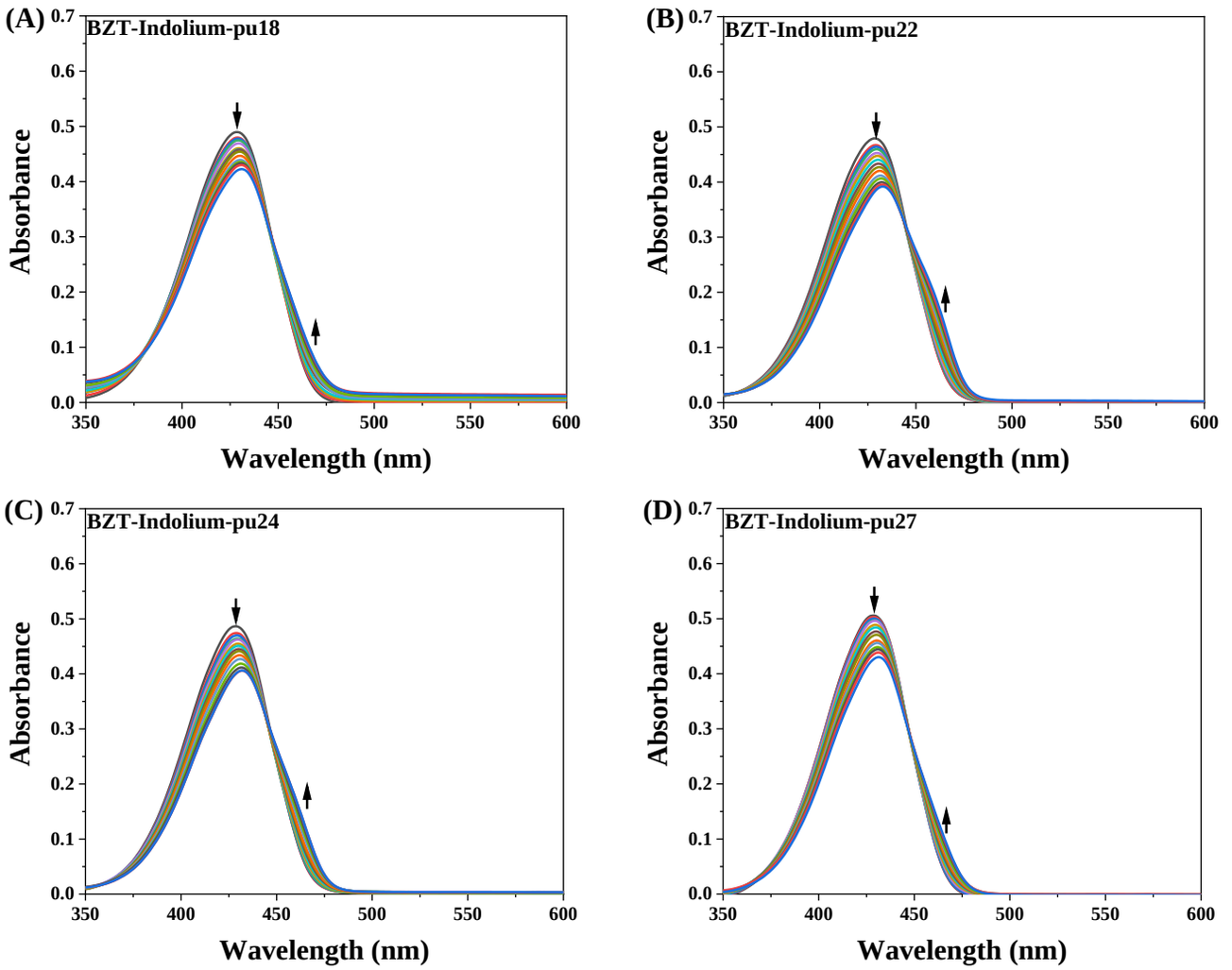

Figure S8. UV-vis titration spectra of **BZT-Indolium** (10 μM) with different concentration of c-MYC G4-DNA in a Tris-HCl buffer (10 mM, pH = 7.4) with 60 mM KCl: (A) pu18; (B) pu22; (C) pu24; and (D) pu27.

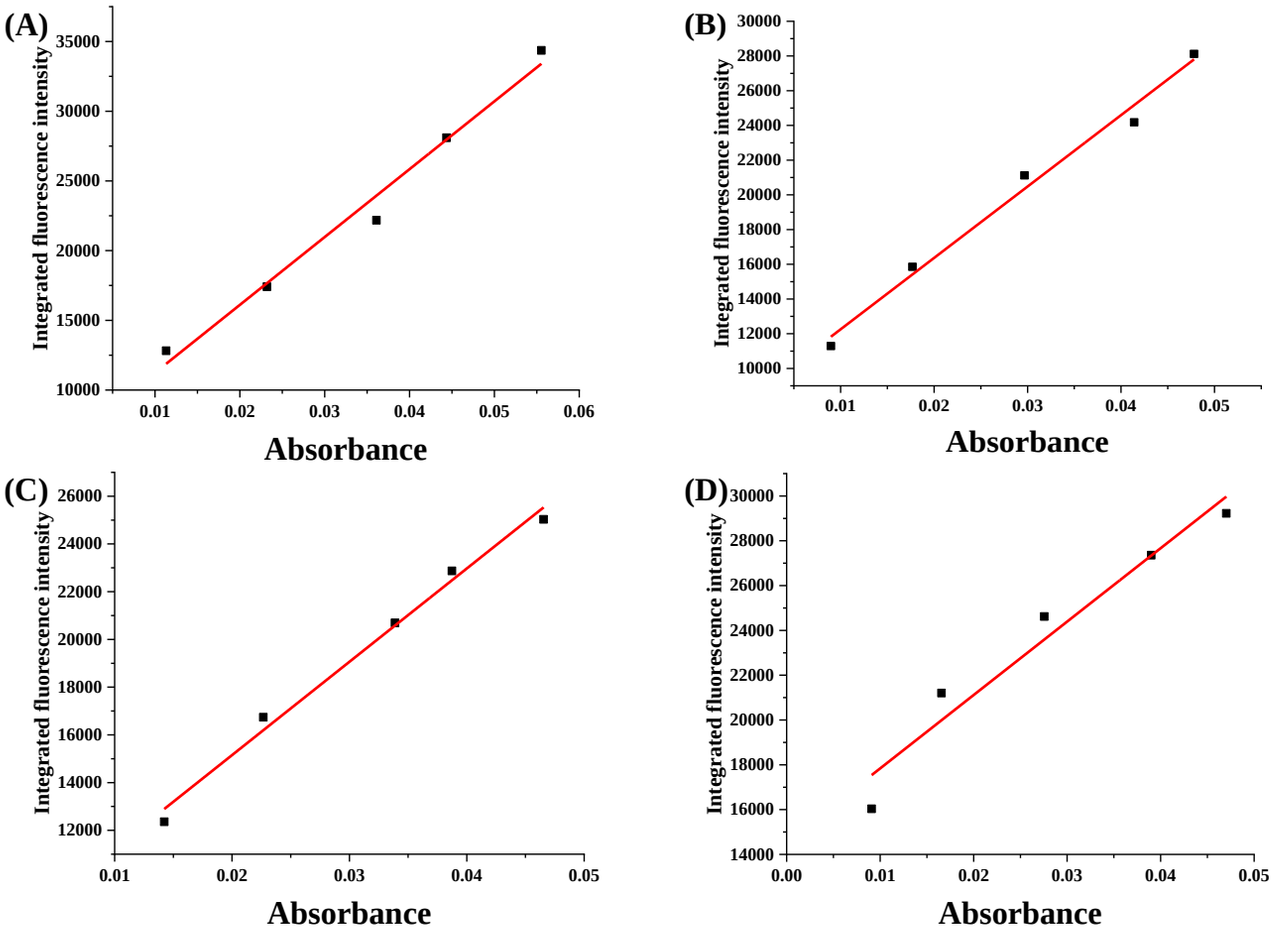

Figure S9. (A) The linear fitting of the absorption intensity by the fluorescence emission spectral integral area of **BZT-Indolium** in pu18; (B) The linear fitting of the absorption intensity by the fluorescence emission spectral integral area of **BZT-Indolium** in pu22; (C) The linear fitting of the absorption intensity by the fluorescence emission spectral integral area of **BZT-Indolium** in pu24; (D) The linear fitting of the absorption intensity by the fluorescence emission spectral integral area of **BZT-Indolium** in pu27. The concentration of **BZT-Indolium** was 0.5 μM in Tris−HCl buffer (10 mM, pH 7.4) containing 60 mM KCl.

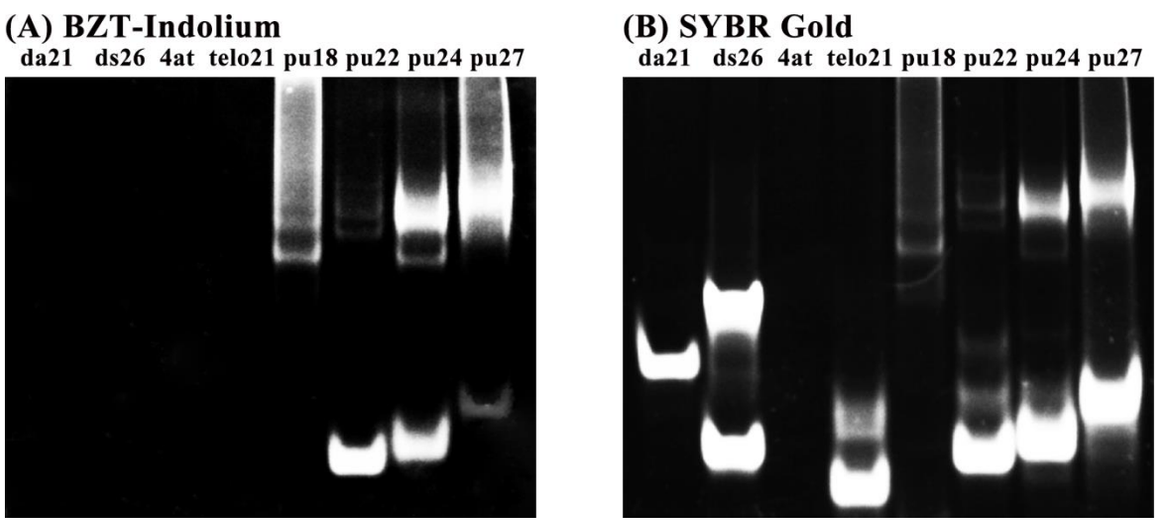

Figure S10. (A) Gel electrophoresis (20 % acrylamide in 1 × TBE) of da21, ds26, 4at, telo21, pu18, pu22, pu24, pu27 at a concentration of 5.0 μM and was stained with **BZT-Indolium** (5.0 μM) for 15 min; (B) Gel electrophoresis (20 % acrylamide in 1 × TBE) of da21, ds26, 4at, telo21, pu18, pu22, pu24, pu27 at a concentration of 5.0 μM and was stained with **SYBR Gold** (5.0 μM) for 15 min.

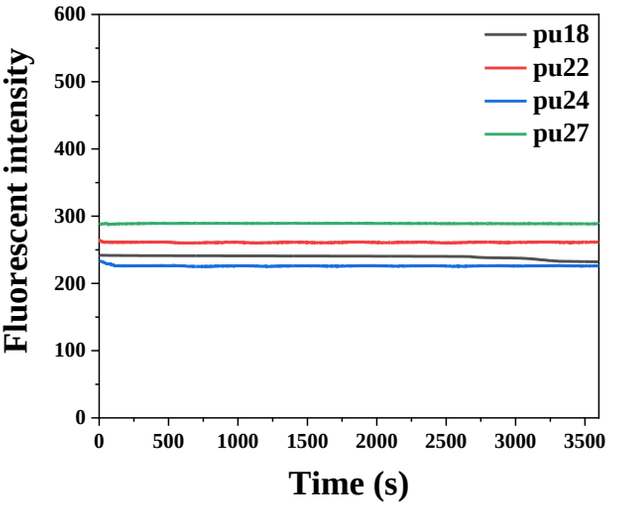

Figure S11. The curve of fluorescence intensity with time (1 h) after the combination of probe **BZT-Indolium** (0.5 μM) with c-MYC promoter G4-DNA (pu18, pu22, pu24, pu27) (1.0 μM). The excitation wavelength λ_{ex} = 434 nm, the emission wavelength λ_{em} = 477 nm.

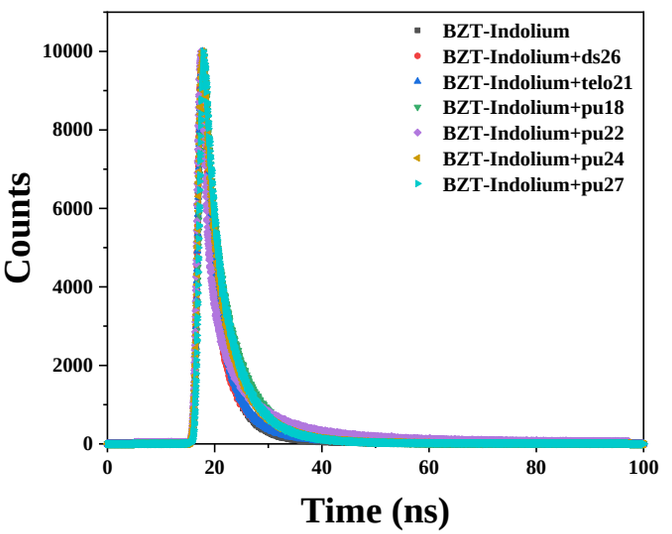

DNA-Probe complex	τ1 (ns)	τ2 (ns)	lifetime (ns)
BZT-Indolium (control)	2.06	5.08	**3.05**
Duplex DNA (ds26)	2.28	9.32	3.28
Telomere G4-DNA (telo21)	2.51	7.26	3.42
c-MYC G4-DNA (pu18)	2.12	6.18	**4.49**
c-MYC G4-DNA (pu22)	2.08	6.32	**4.07**
c-MYC G4-DNA (pu24)	2.39	6.20	**4.12**
c-MYC G4-DNA (pu27)	2.13	5.72	**4.20**

Figure S12. Fluorescence decay traces of **BZT-Indolium** (0.5 μM, λ_{ex} = 320 nm, λ_{em} = 477 nm) in the absence and in the presence of different DNA substrates including ds26, telo21, pu18, pu22, pu24 and pu27 in 10 mM Tris-HCl buffer at pH 7.4 containing 60 mM KCl.

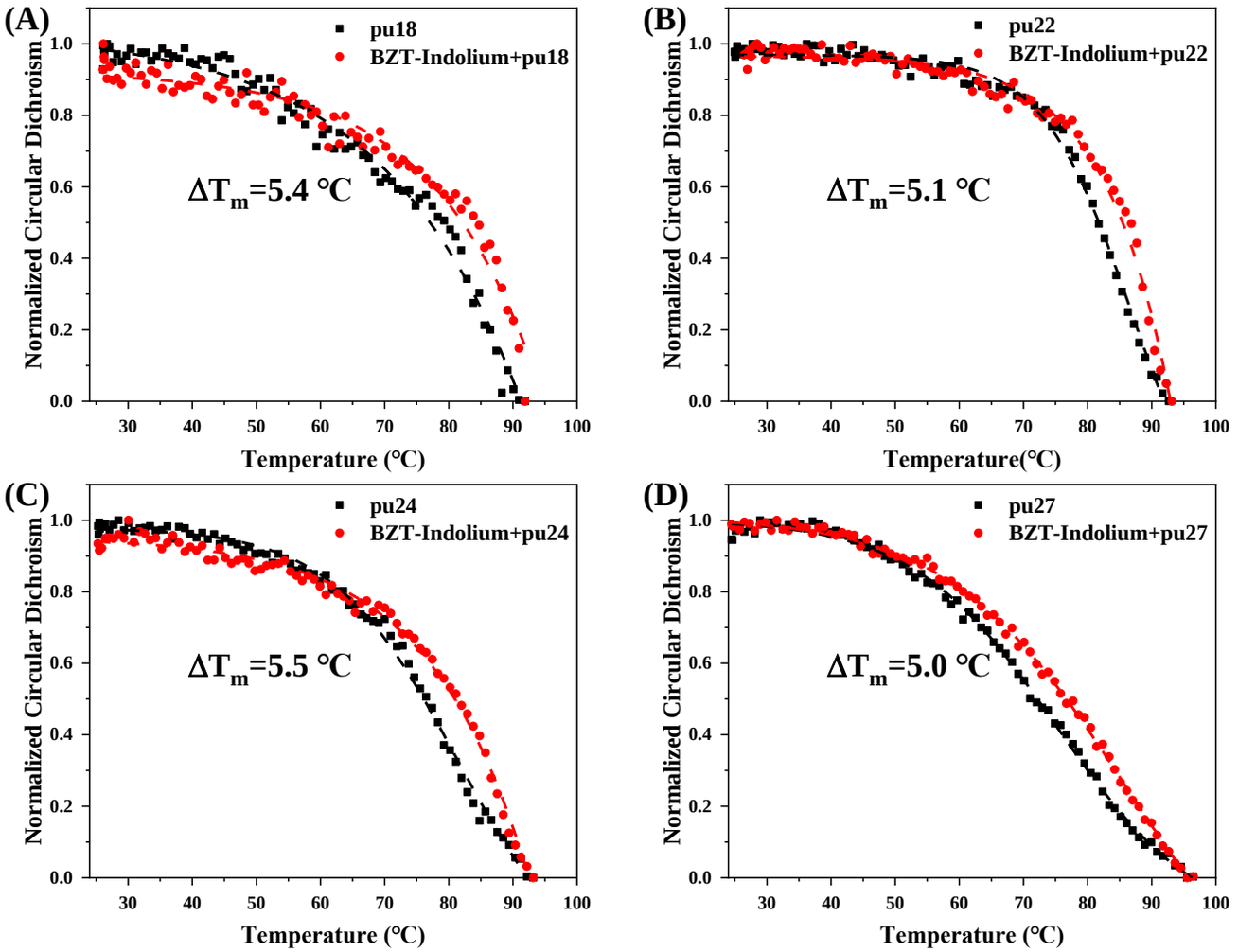

Figure S13. The evaluation the G4-structure stabilization ability of **BZT-Indolium** in 10 mM Tris-HCl buffer at pH 7.4 containing 60 mM KCl: (A) Normalized CD signal of pu18 during melting process; (B) Normalized CD signal of pu22 during melting process; (C) Normalized CD signal of pu24 during melting process; (D) Normalized CD signal of pu27 during melting process. The G-quadruplex was characterized by the positive peak at 262 nm.

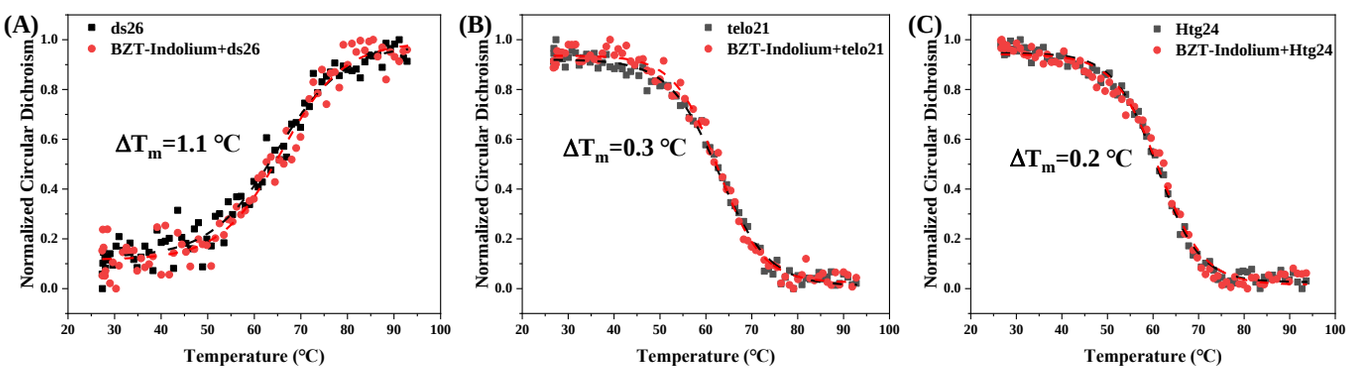

Figure S14. The evaluation the stabilization ability of **BZT-Indolium** in 10 mM Tris-HCl buffer at pH 7.4 containing 60 mM KCl: (A) Normalized CD signal of double stranded DNA (ds26) during melting process, the double stranded DNA was characterized by the negative peak at 242 nm; (B) Normalized CD signal of Telomere G4-DNA (telo21) during melting process, the G-quadruplex was characterized by the positive peak at 290 nm; (C) Normalized CD signal of Telomere G4-DNA (Htg24) during melting process, the G-quadruplex was characterized by the positive peak at 290 nm.

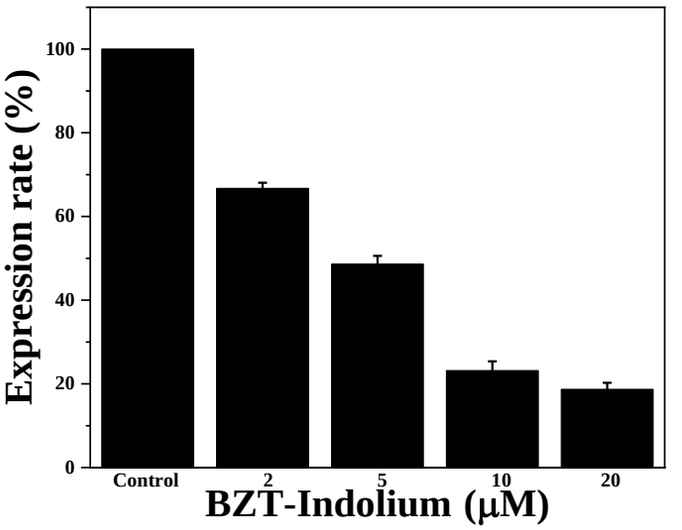

Figure S15. Expression rate of c-MYC mRNA at different concentrations of **BZT-Indolium**.

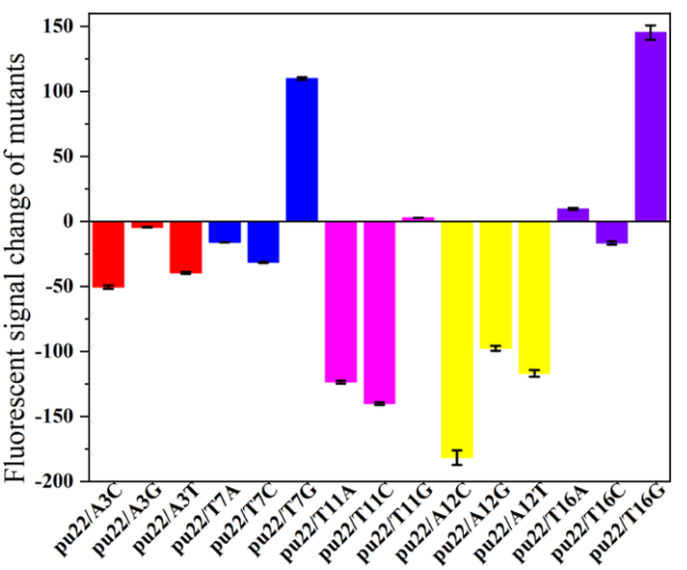

Figure S16. Fluorescence binding assays of **BZT-Indolium** with pu22 mutants in Tris–HCl buffer containing 60 mM KCl. Fluorescence signal change = F_{pu22} mutant-F_{pu22} wild type.

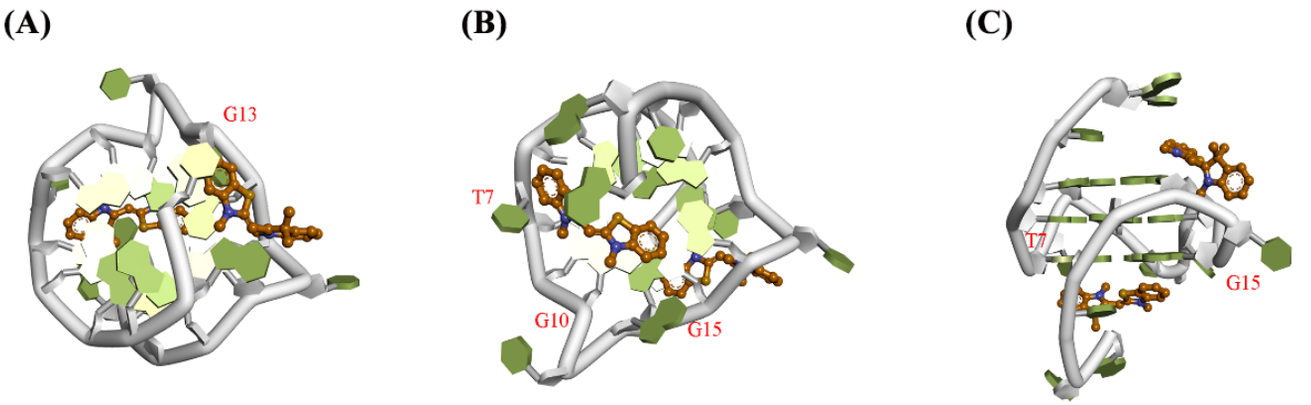

Figure S17. The molecular docking study of **BZT-Indolium** in complex with pu22 G-quadruplex. Top view (A), bottom view (B) and side view (C) of **BZT-Indolium** in complex with pu22 G-quadruplex in a 2:1 binding mode. Residues involved in the ligand-G4 interactions were highlighted.

The molecular docking results of **BZT-Indolium** in complex with pu22 G-quadruplex in 2:1 binding mode were shown in **Figure S17**. At the 5' end planar, the benzothiazole scaffold of **BZT-Indolium** is able to stack on the pu22 G4 mainly by pi-pi stacking with G13 and T1 residues, while the methylquinolinium with two methyl group is pointing out of the G4 structure. At the 3' end planar, the benzothiazole group is pi-pi stacking with G10 and G15 residues, while the methylquinolinium structure is pi-pi stacking with T7 loop. The result of molecular docking is consistent with the NMR titration and fluorescence binding assays.

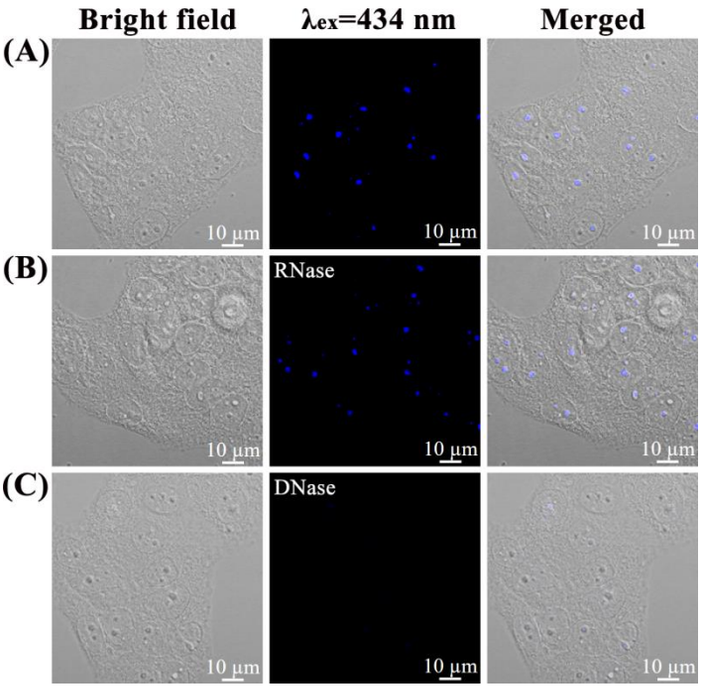

Figure S18. (A) Fluorescence images of live MCF-7 cells stained with 5.0 μM **BZT-Indolium** for 15 min; (B) Fluorescence images of live MCF-7 cells stained with 5.0 μM **BZT-Indolium** for 15 min and RNase treated for 2 h; (C) Fluorescence images of live MCF-7 cells stained with 5 μM **BZT-Indolium** for 15 min and DNase treated for 2 h.

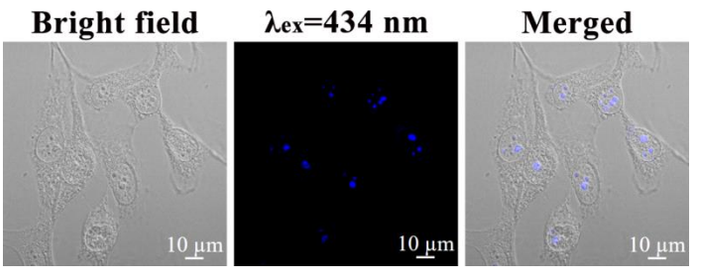

Figure S19. Fluorescence images of live non-cancer cells 16HBE stained with 5.0 μM **BZT-Indolium** for 15 min.

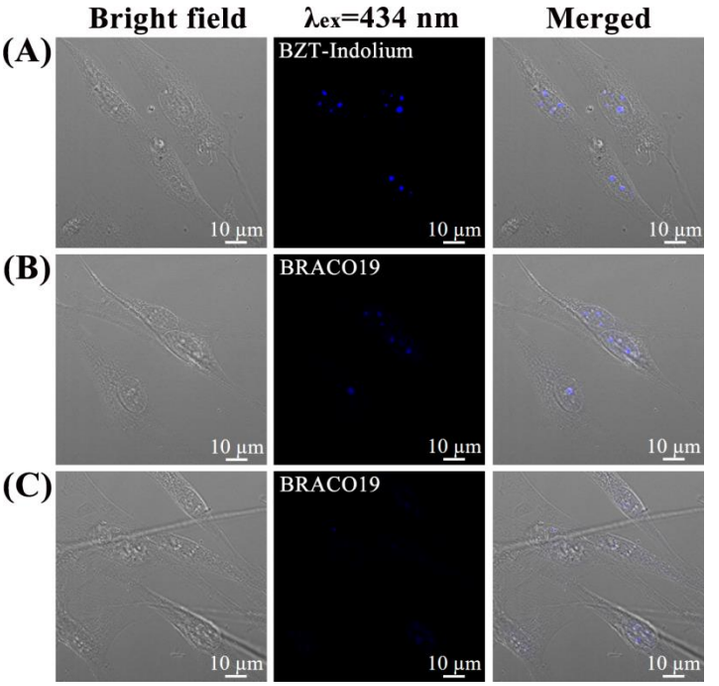

Figure S20. Intracellular competition experiments in live U87 cells and images were taken after incubated for 15 min: (A) 5 μM probe; (B) 5 μM probe and then 5 μM BRACO19; (C) 5 μM probe and then 10 μM BRACO19.

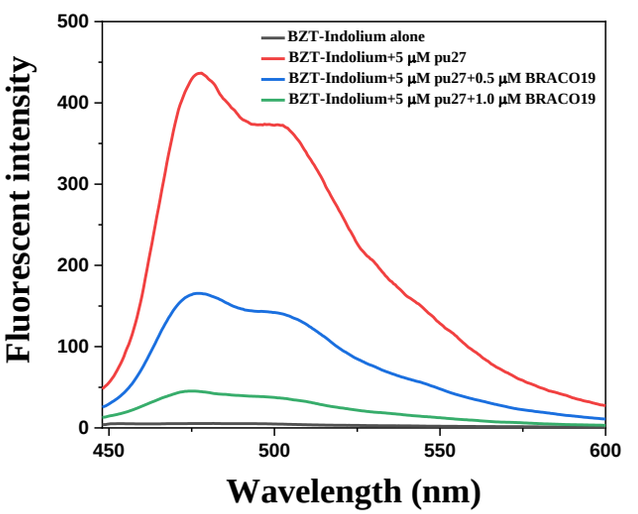

Figure S21. Fluorescence response of **BZT-Indolium** (0.5 μM) added to pu27 G4-DNA and BRACO19 was added subsequently. The concentration ratio between **BZT-Indolium** and BRACO19 is 1: 1 and 1: 2.

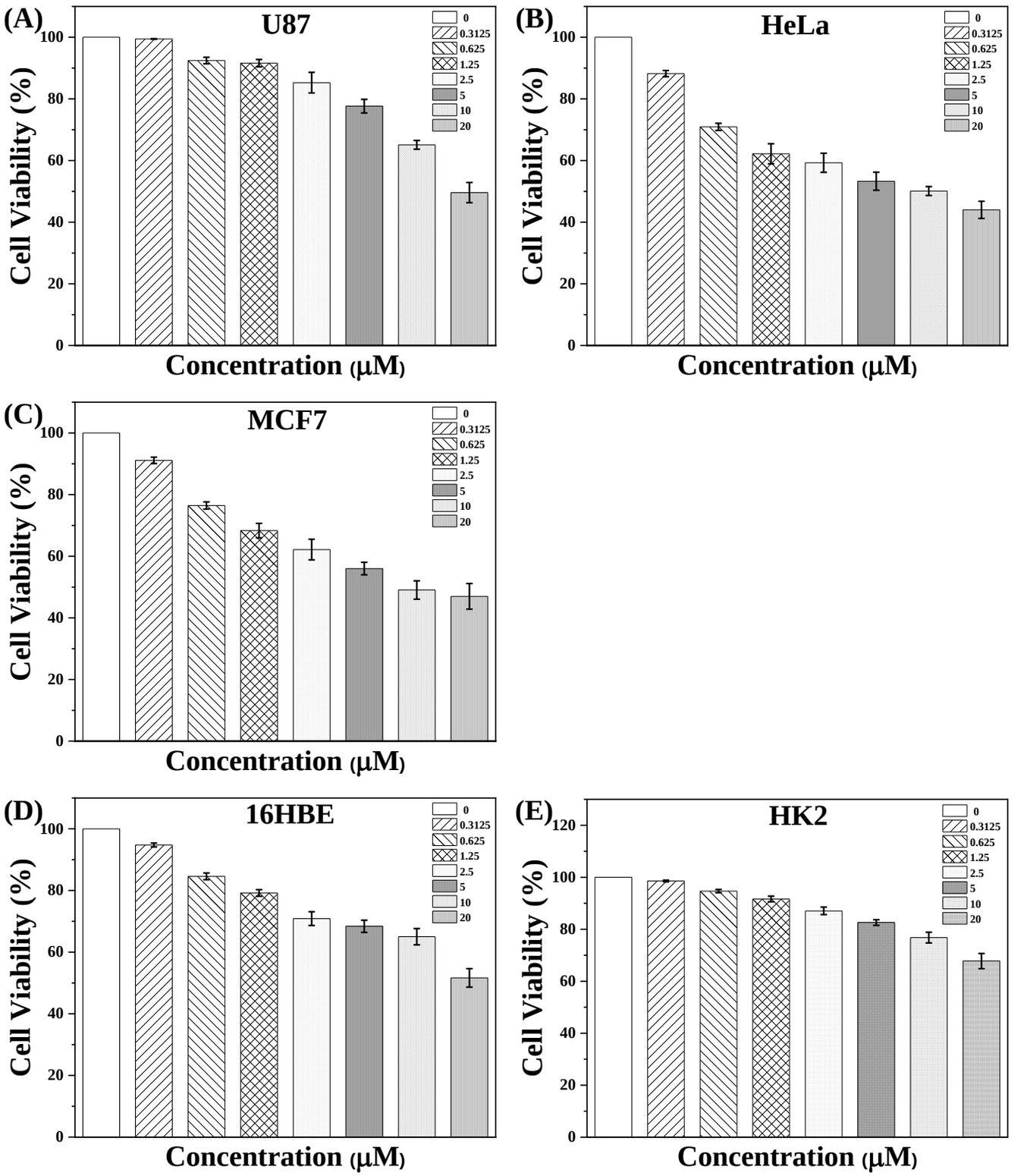

Figure S22. (A) Cells survival viability of U87 cells; (B) Cells survival viability of HeLa cells; (C) Cells survival viability of MCF7 cells; (D) Cells survival viability of 16HBE cells; (E) Cells survival viability of HK2 cells. The concentration gradients of **BZT-Indolium** were 0, 0.3125, 0.625, 1.25, 5, 10 and 20 μM.

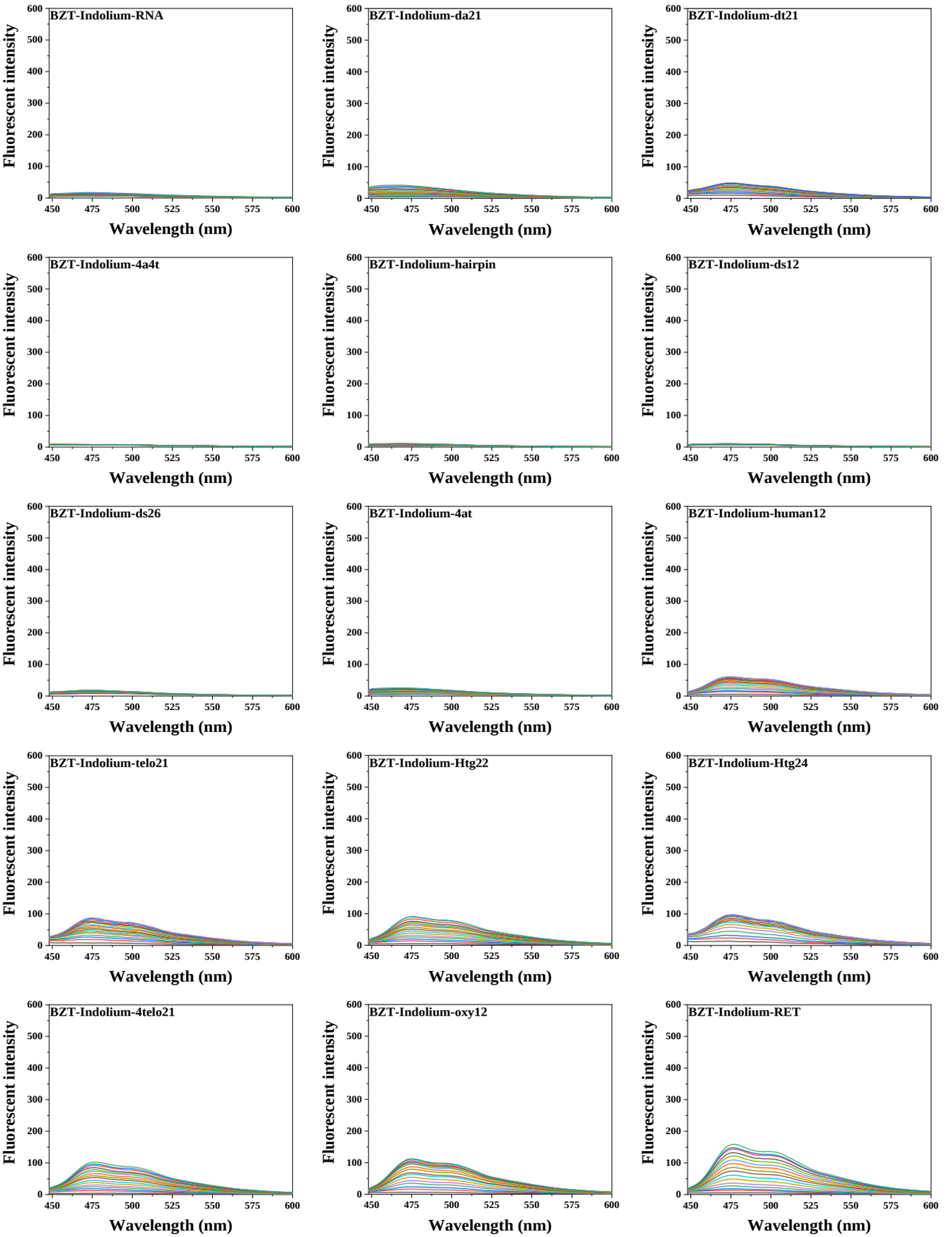
BZT-Indolium-RNA
BZT-Indolium-da21
BZT-Indolium-dt21
BZT-Indolium-4a4t
BZT-Indolium-hairpin
BZT-Indolium-ds12
BZT-Indolium-ds26
BZT-Indolium-4at
BZT-Indolium-human12
BZT-Indolium-telo21
BZT-Indolium-Htg22
BZT-Indolium-Htg24
BZT-Indolium-4telo21
BZT-Indolium-oxy12
BZT-Indolium-RET
Fluorescent intensity
Wavelength (nm)
0
100
200
300
400
500
600
450
475
500
525
550
575
600

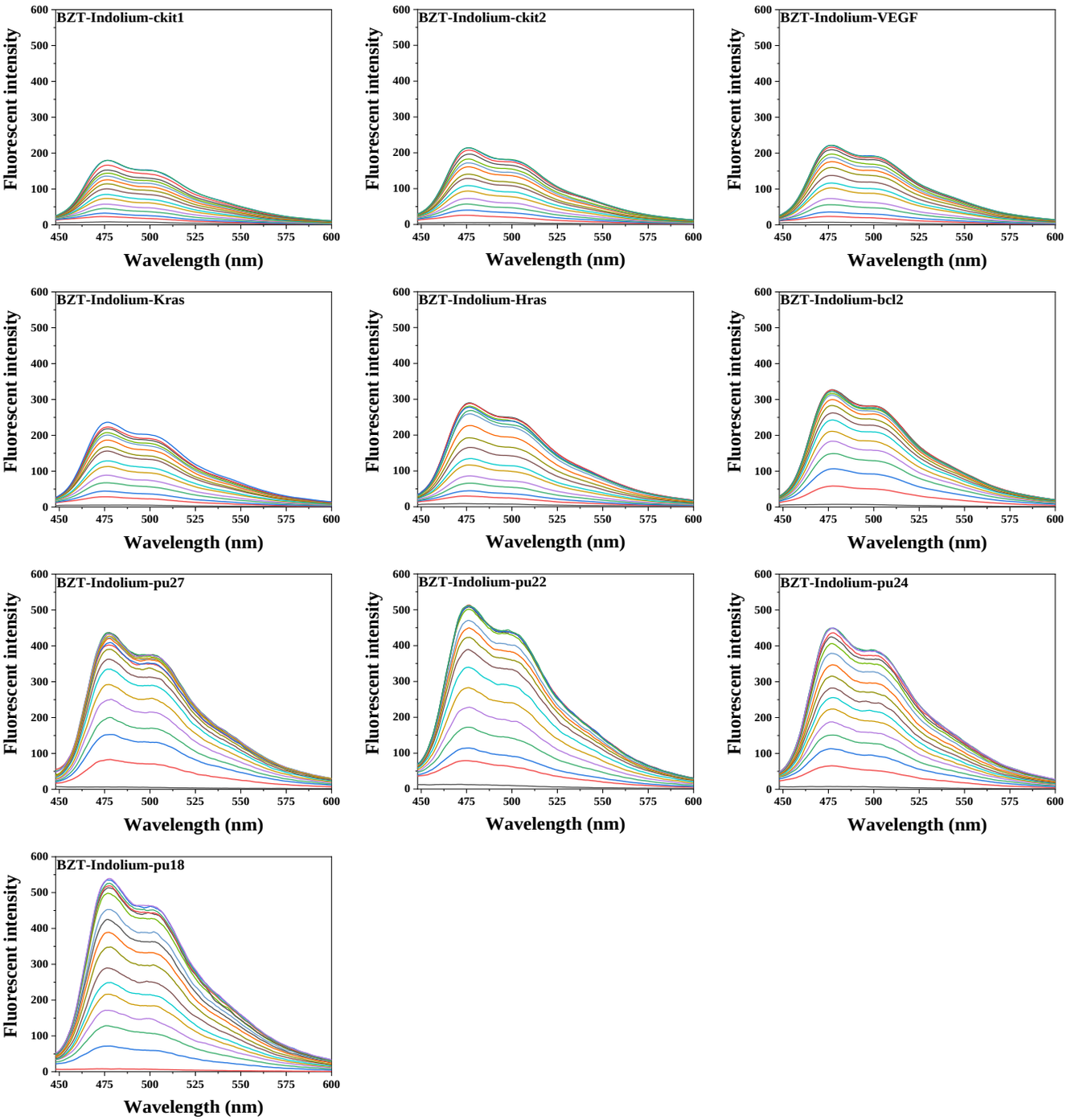

Figure S23. Fluorescence titration spectra of **BZT-Indolium** with different nucleic acids: RNA; single-stranded DNA: da21, dt21; duplex DNA: 4a4t, hairpin, ds12, ds26, 4at; Telomere G4-DNA: human12, telo21, Htg22, Htg24, 4telo21, oxy12; Promoter G4-DNA: RET, ckit1, ckit2, VEGF, Kras, Hras, bcl2, pu18, pu22, pu24 and pu27 in a Tris-HCl buffer (10 mM, pH 7.4) containing 60 mM KCl. Fluorescence signal was measured at 25 °C.

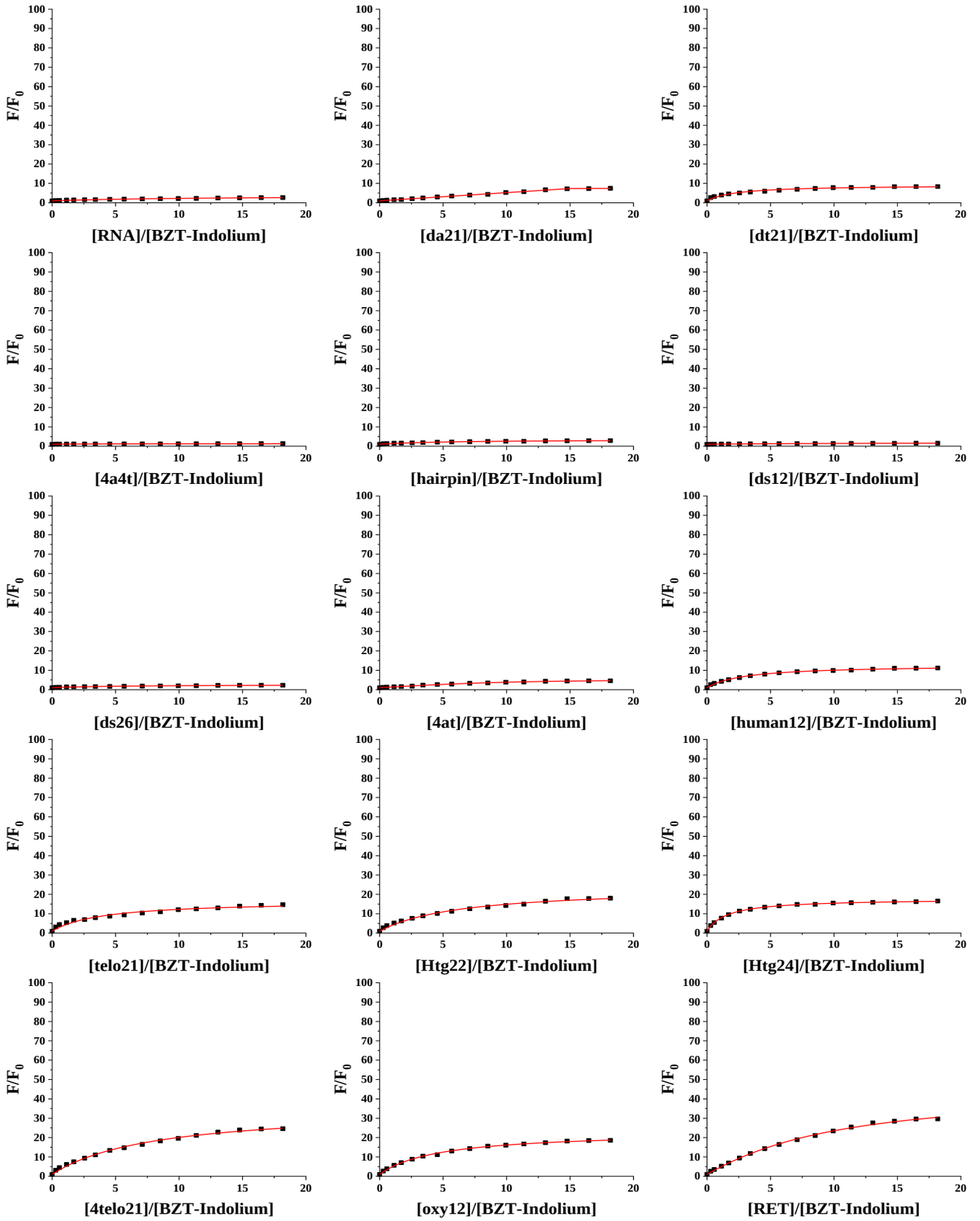
F/F0
[RNA]/[BZT-Indolium]
[da21]/[BZT-Indolium]
[dt21]/[BZT-Indolium]
[4a4t]/[BZT-Indolium]
[hairpin]/[BZT-Indolium]
[ds12]/[BZT-Indolium]
[ds26]/[BZT-Indolium]
[4at]/[BZT-Indolium]
[human12]/[BZT-Indolium]
[telo21]/[BZT-Indolium]
[Htg22]/[BZT-Indolium]
[Htg24]/[BZT-Indolium]
[4telo21]/[BZT-Indolium]
[oxy12]/[BZT-Indolium]
[RET]/[BZT-Indolium]

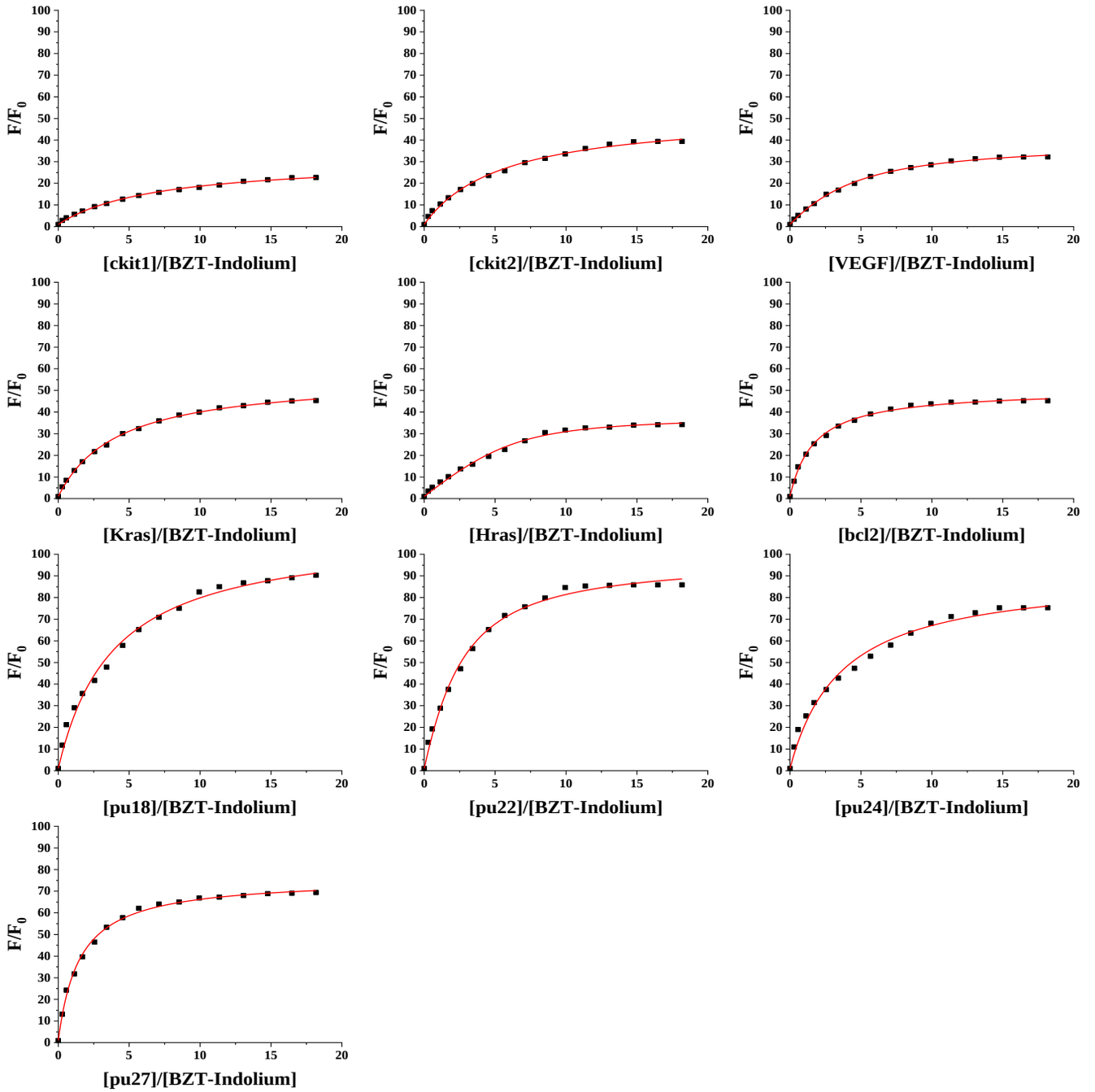

Figure S24. Fluorescence titrations, presented as a relative increase of the integral fluorescence (F/F_0) of different nucleic acids: RNA; single-stranded DNA: da21, dt21; duplex DNA: 4a4t, hairpin, ds12, ds26, 4at; Telomere G4-DNA: human12, telo21, Htg22, Htg24, 4telo21, oxy12; Promoter G4-DNA: RET, ckit1, ckit2, VEGF, Kras, Hras, bcl2, pu18, pu22, pu24 and pu27 with **BZT-Indolium** (0.5 μM) in 10 mM Tris-HCl buffer (pH 7.4, containing 60 mM KCl).

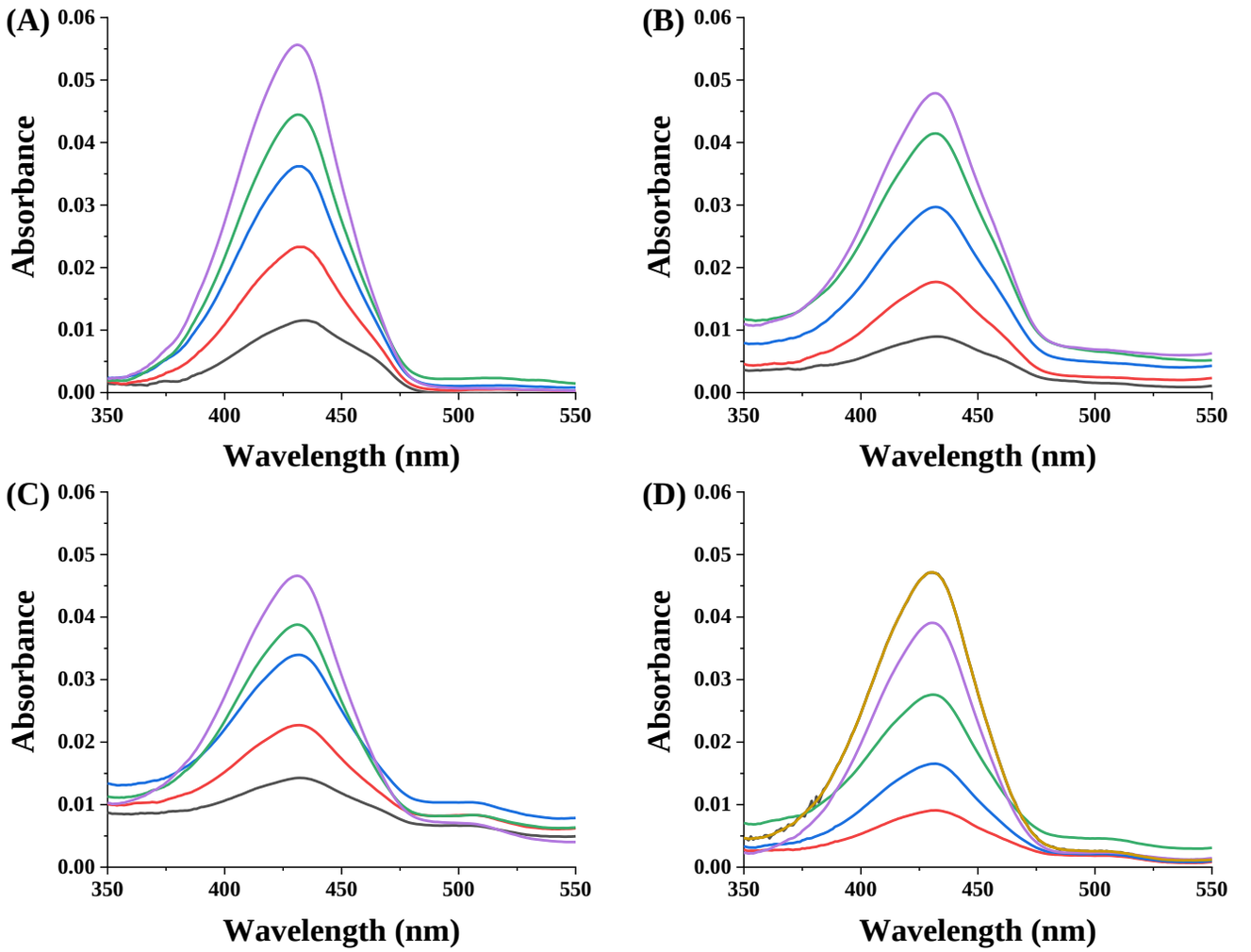

Figure S25. (A) The UV absorption spectrum obtained by adding five continuous concentrations (0.4 μM, 0.8 μM, 1.2 μM, 1.6 μM ,2.0 μM) of **BZT-Indolium** to a fixed concentration of 1 μM pu18; (B) The UV absorption spectrum obtained by adding five continuous concentrations (0.4 μM, 0.8 μM, 1.2 μM, 1.6 μM ,2.0 μM) of **BZT-Indolium** to a fixed concentration of 1 μM pu22; (C) The UV absorption spectrum obtained by adding five continuous concentrations (0.4 μM, 0.8 μM, 1.2 μM, 1.6 μM ,2.0 μM) of **BZT-Indolium** to a fixed concentration of 1 μM pu24; (D) The UV absorption spectrum obtained by adding five continuous concentrations (0.4 μM, 0.8 μM, 1.2 μM, 1.6 μM ,2.0 μM) of **BZT-Indolium** to a fixed concentration of 1 μM pu27.

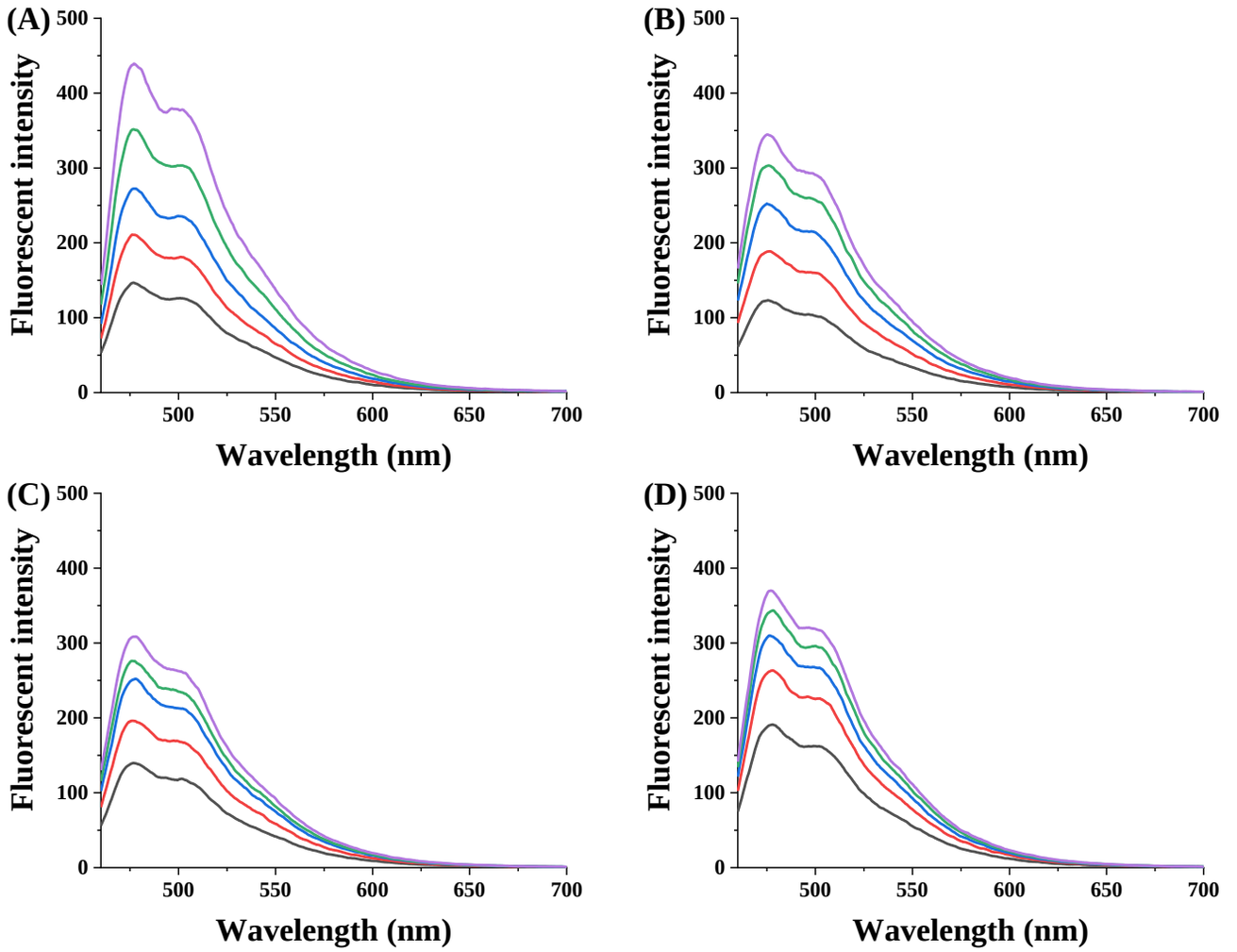

Figure S26. (A) Fluorescence spectrum obtained by adding five continuous concentrations of **BZT-Indolium** (0.4 μM, 0.8 μM, 1.2 μM, 1.6 μM ,2.0 μM) to a fixed concentration of 1 μM pu18; (B) Fluorescence spectrum obtained by adding five continuous concentrations of **BZT-Indolium** (0.4 μM, 0.8 μM, 1.2 μM, 1.6 μM ,2.0 μM) to a fixed concentration of 1 μM pu22; (C) Fluorescence spectrum obtained by adding five continuous concentrations of **BZT-Indolium** (0.4 μM, 0.8 μM, 1.2 μM, 1.6 μM ,2.0 μM) to a fixed concentration of 1 μM pu24; (D) Fluorescence spectrum obtained by adding five continuous concentrations (0.4 μM, 0.8 μM, 1.2 μM, 1.6 μM ,2.0 μM) of **BZT-Indolium** to a fixed concentration of 1 μM pu27.

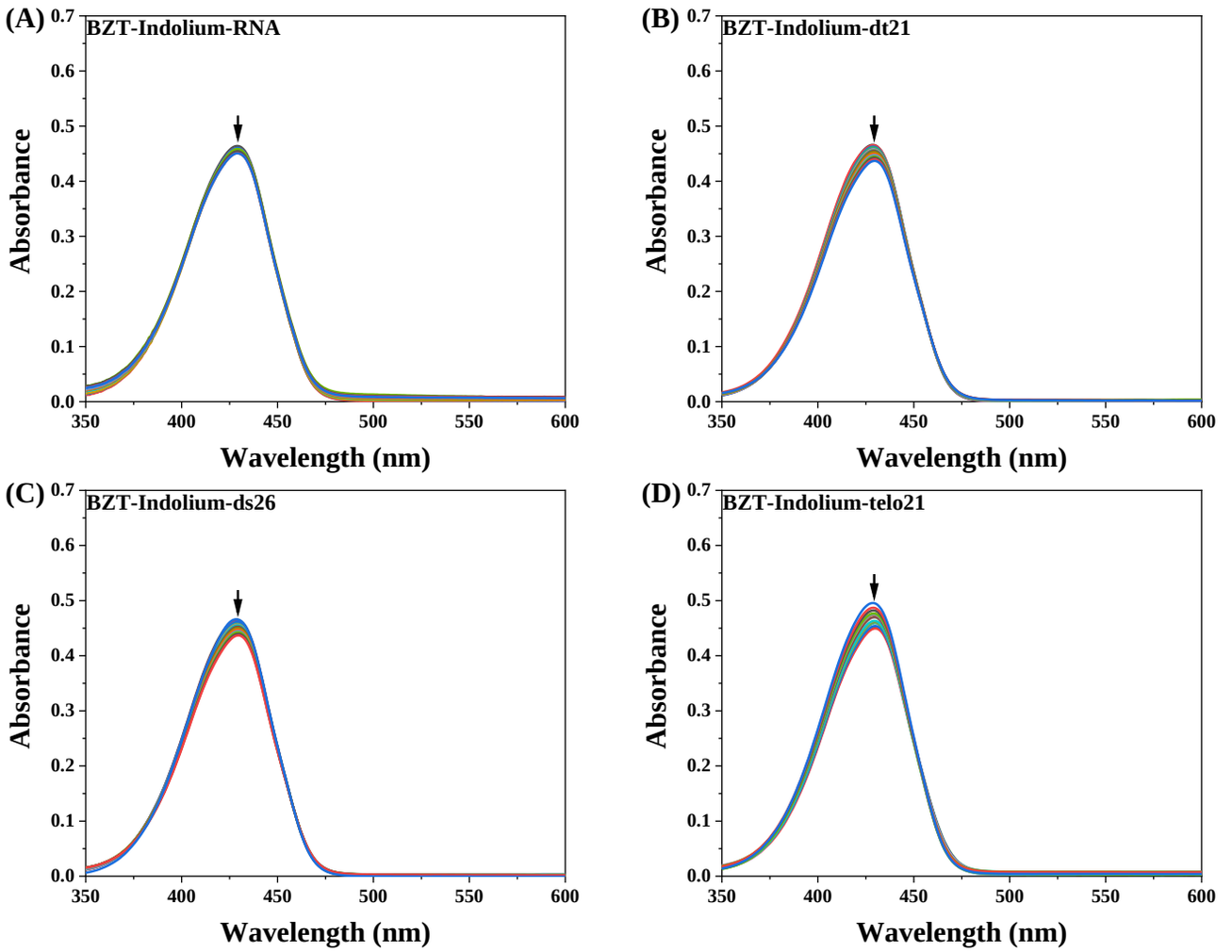

Figure S27. UV-vis titration spectra of **BZT-Indolium** (10 μM) with selected nucleic acids in a Tris-HCl buffer (10 mM, pH = 7.4) with 60 mM KCl at 25 °C: (A) RNA. (B) dt21. (C) ds26. (D) telo21 G4-DNA.

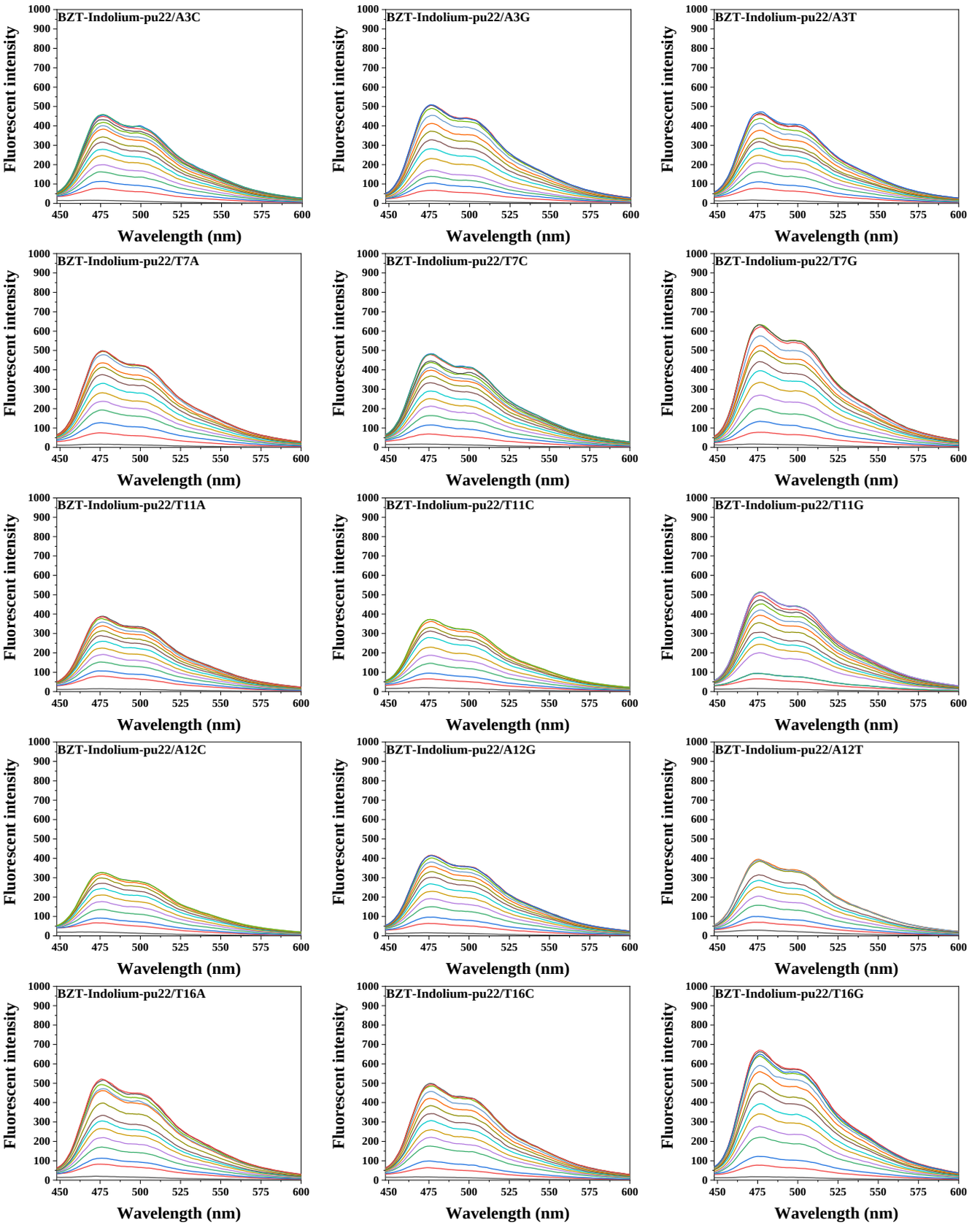

Figure S28. Fluorescence titration spectra of **BZT-Indolium** with different concentrations of pu22 mutants. The concentration of **BZT-Indolium** was 0.5 μM in Tris−HCl buffer (10 mM, pH 7.4) containing 60 mM KCl.

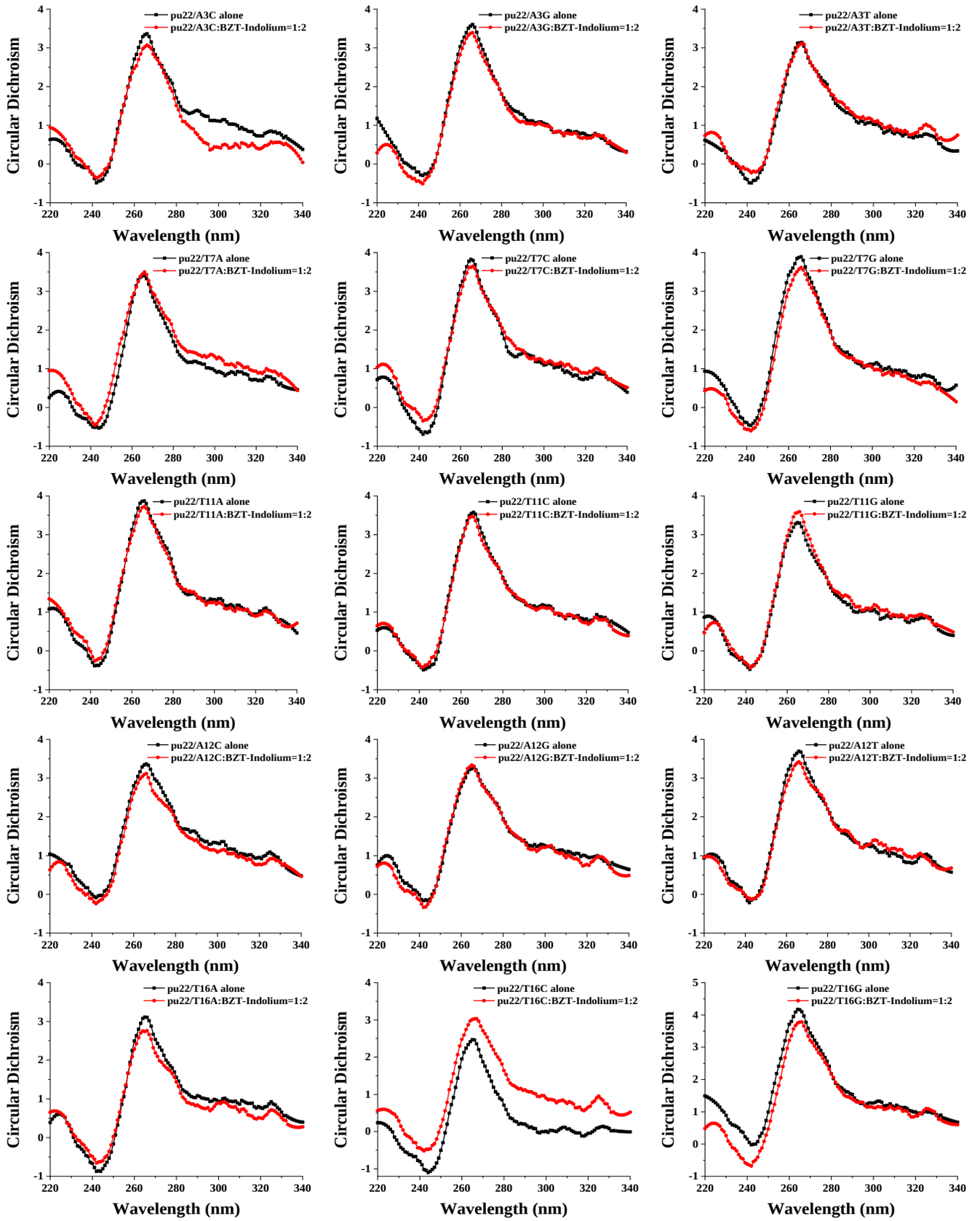

Figure S29. CD spectra of 5 μM pu22/A3C, pu18/A3G, pu22/A3T, pu22/T7A, pu22/T7C, pu22/T7G, pu22/T11A, pu22/T11C, pu22/T11G, pu22/A12C, pu22/A12G, pu22/A12T, pu22/T16A, pu22/T16C, pu22/T16G binding to **BZT-Indolium** in 10 mM Tris-HCl buffer at pH 7.4 with 60 mM KCl.

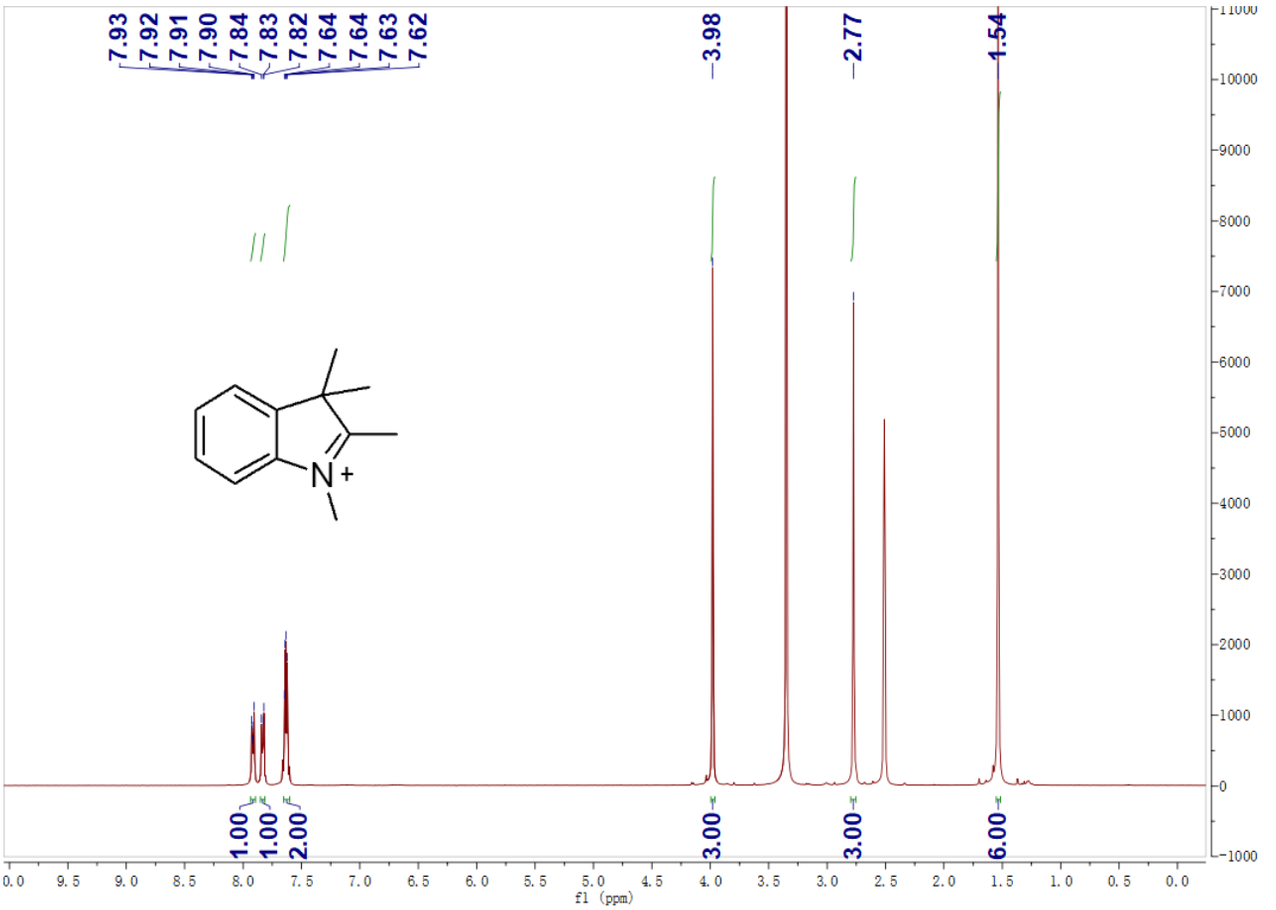

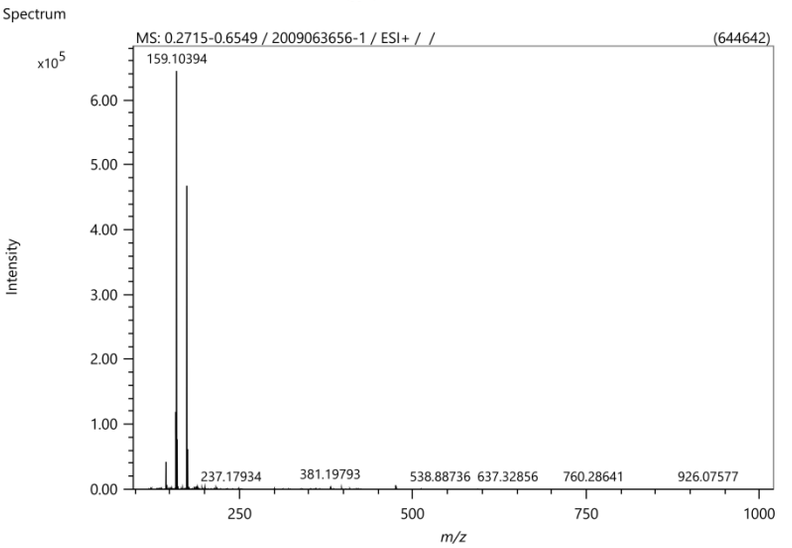

Elemental Composition

Parameters		Elements Set 1:							
Tolerance:	±5.00 ppm	Symbol	C	H	N	O	Na	S	Cl	Br
Electron:	Odd/Even	Min	0	0	0	0	0	0	0	0
Charge:	+1	Max	200	200	4	8	0	0	0	0
DBE:	-1.5 - 200.0									

Symbol	F	Si
Min	0	0
Max	0	0

Results

Mass	Intensity	Intensity [%]	Formula	Calculated Mass	Mass Difference [mDa]	Mass Difference [ppm]	DBE
174.12794	467889.18	72.58	C12 H16 N	174.12773	0.22	1.24	5.5

Figure S30. ^{1}H NMR (DMSO-d_6), HRMS of intermediate **A**.

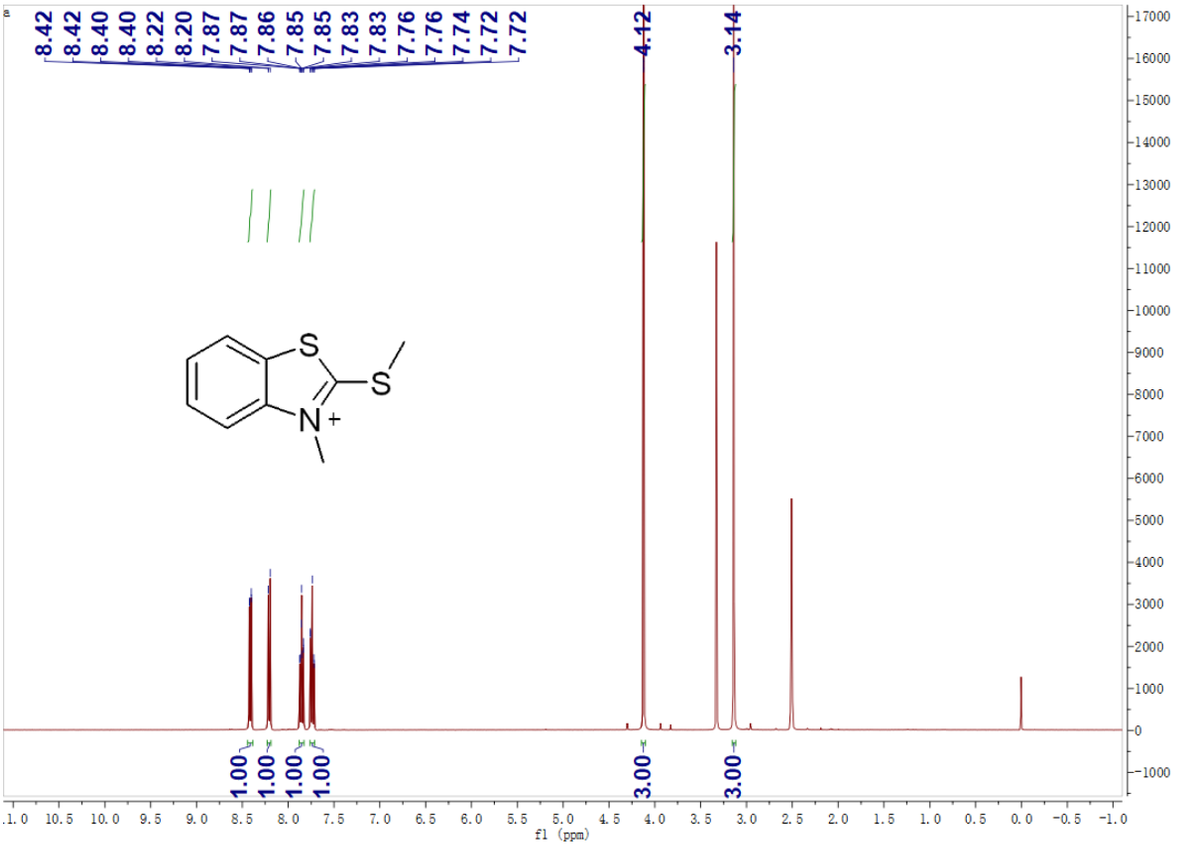

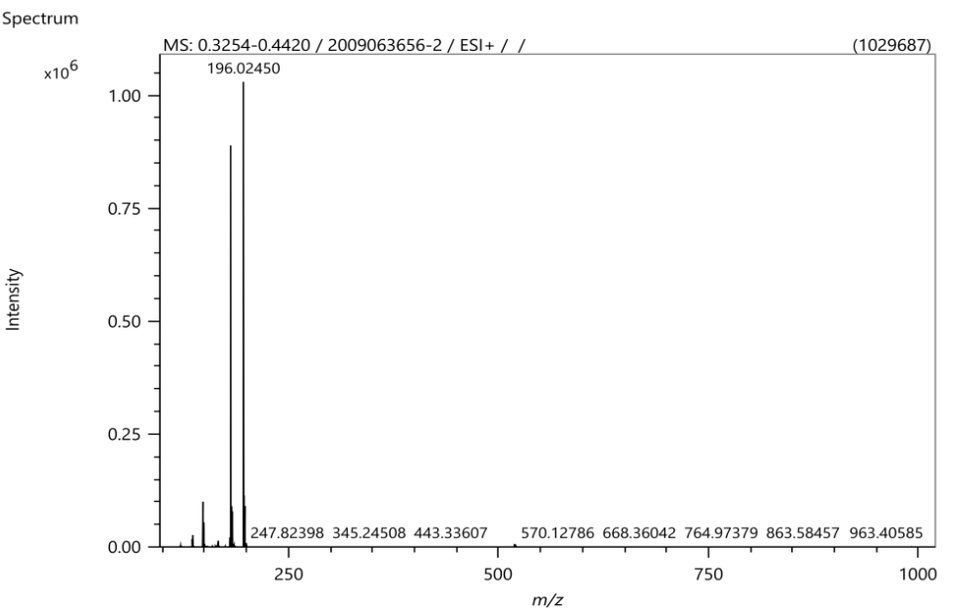

Elemental Composition

Parameters	
Tolerance:	±5.00 ppm
Electron:	Odd/Even
Charge:	+1
DBE:	-1.5 - 200.0

Elements Set 1:

Symbol	C	H	N	O	Na	S	Cl	Br
Min	0	0	0	0	0	2	0	0
Max	200	200	3	8	0	2	0	0

Symbol	F	Si
Min	0	0
Max	0	0

Results

Mass	Intensity	Intensity [%]	Formula	Calculated Mass	Mass Difference [mDa]	Mass Difference [ppm]	DBE
196.02450	1029686.71	100.00	C9 H10 N S2	196.02492	-0.41	-2.11	5.5

Figure S31. ^{1}H NMR (DMSO-d_6), HRMS of intermediate **B**.

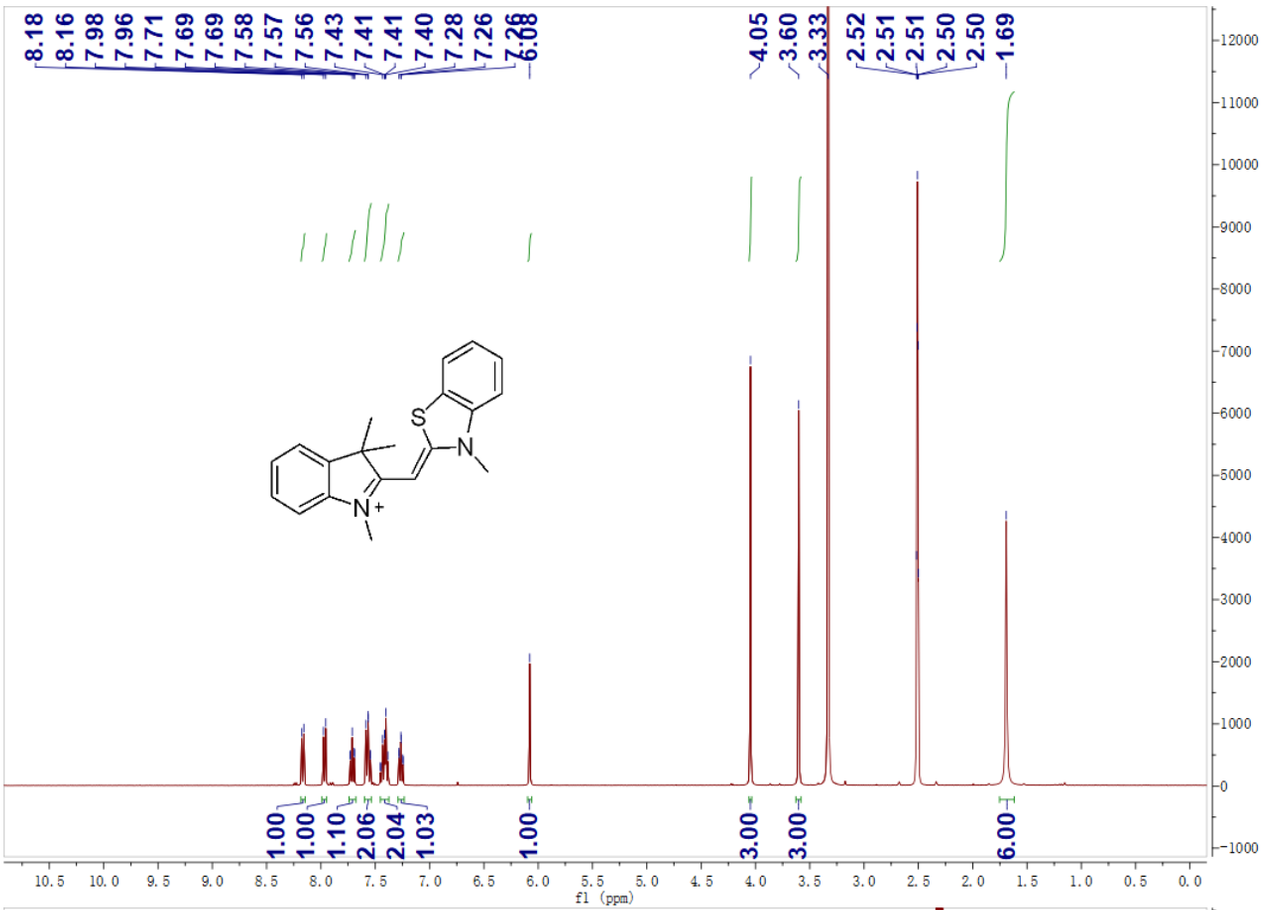
8.18
8.16
7.98
7.96
7.71
7.69
7.69
7.58
7.57
7.56
7.43
7.41
7.41
7.40
7.28
7.26
6.08
4.05
3.60
3.33
2.52
2.51
2.51
2.50
2.50
1.69
1.00
1.00
1.10
2.06
2.04
1.03
1.00
3.00
3.00
6.00
f1 (ppm)

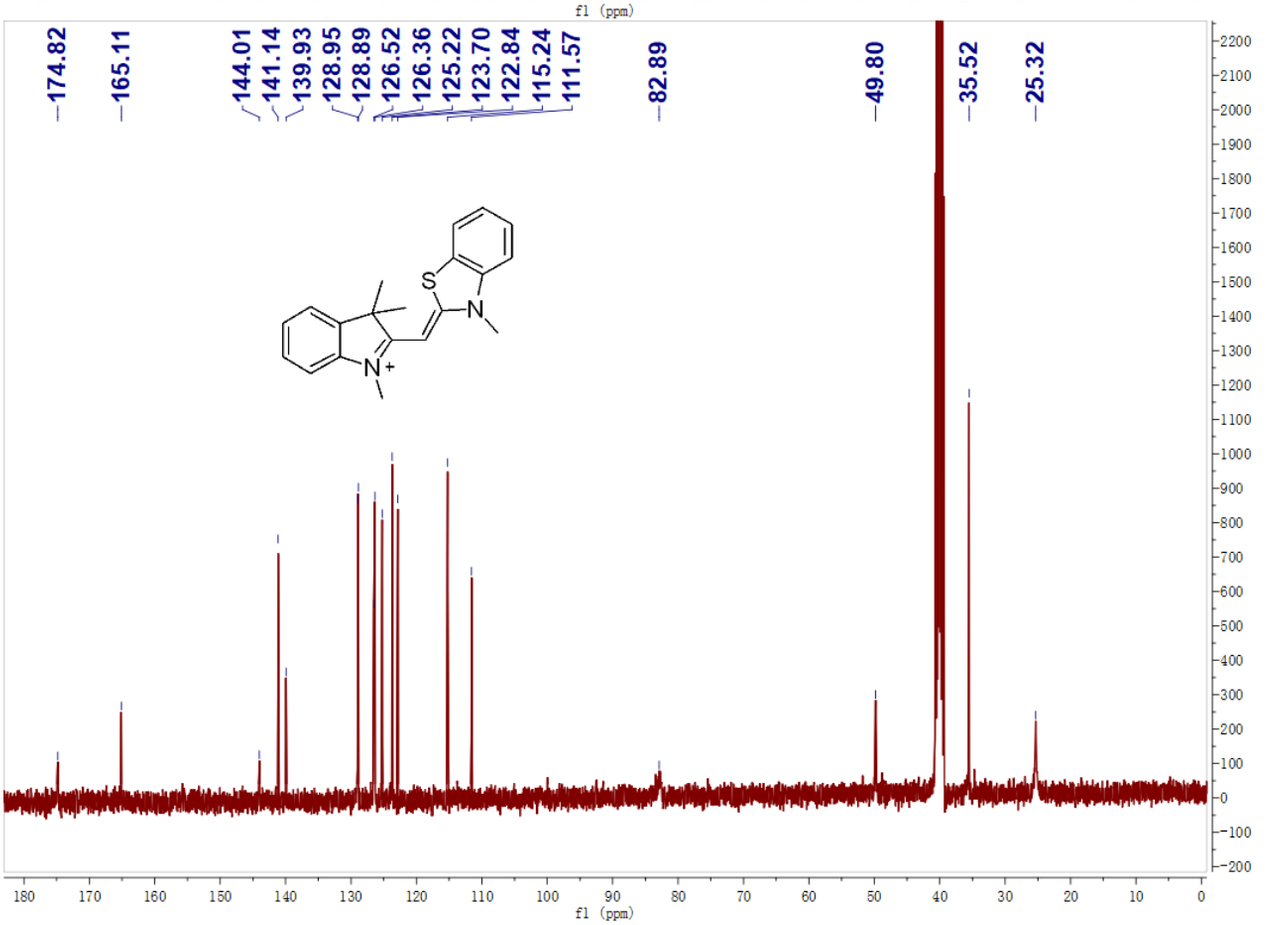
174.82
165.11
144.01
141.14
139.93
128.95
128.89
126.52
126.36
125.22
123.70
122.84
115.24
111.57
82.89
49.80
35.52
25.32
f1 (ppm)

Spectrum

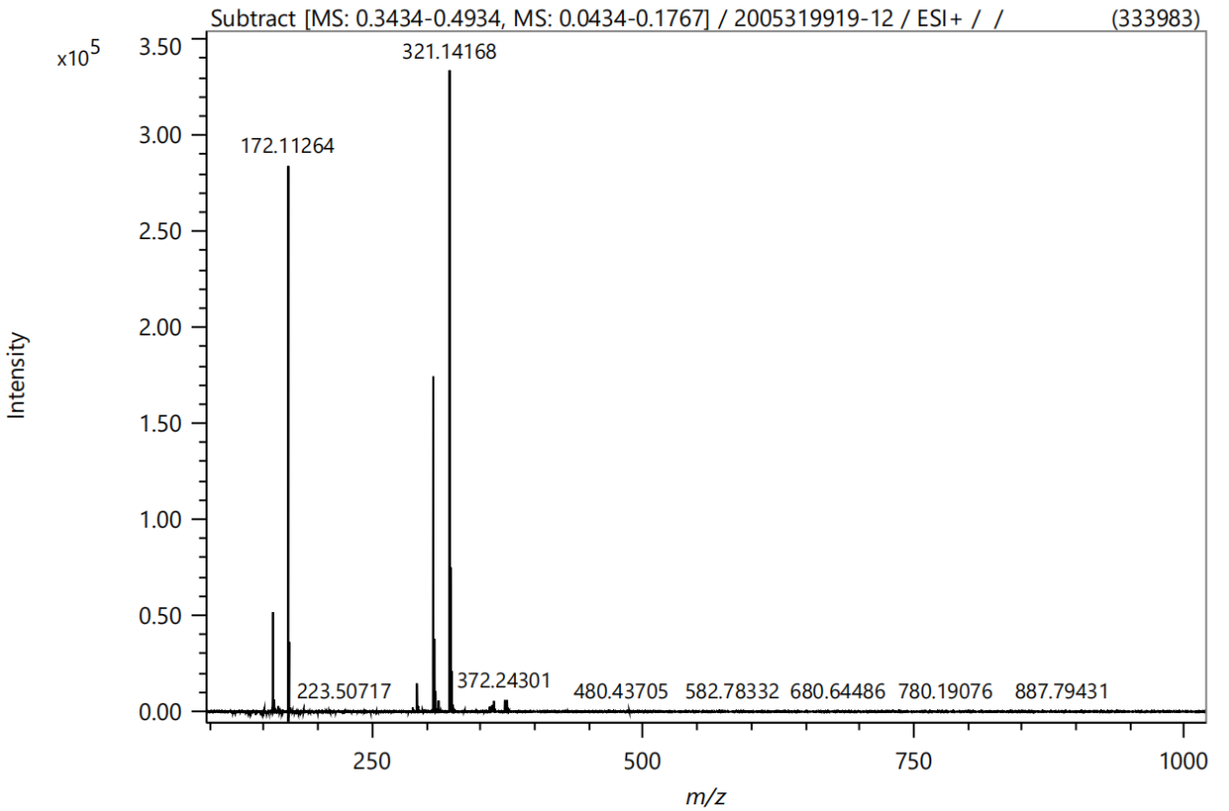

Elemental Composition

Parameters	
Tolerance:	±5.00 ppm
Electron:	Odd/Even
Charge:	+1
DBE:	-1.5 - 200.0

Elements Set 1:

Symbol	C	H	N	O	Na	S	Cl	Br
Min	0	0	0	0	0	1	0	0
Max	120	120	5	10	0	1	0	0

Symbol	F	Si	P	Mn	B	I	Ir
Min	0	0	0	0	0	0	0
Max	0	0	0	0	0	0	0

Results

Mass	Intensity	Intensity [%]	Formula	Calculated Mass	Mass Difference [mDa]	Mass Difference [ppm]	DBE
321.14168	333983.21	100.00	C20 H21 N2 S	321.14200	-0.31	-0.97	11.5

Figure S32. ^{1}H NMR (DMSO-d_6), ^{13}C NMR (DMSO-d_6), HRMS of **BZT-Indolium**.

Reference

1. G. M. Morris, R. Huey, W. Lindstrom, M. F. Sanner and A. J. Olson, *J. Comput. Chem.*, 2009, **30**, 2785–2791.
2. A. M. Brouwer, *Pure Appl. Chem.*, 2011, **83**, 2213–2228.
3. R. S. Tuma, M. P. Beaudet, X. Jin, L. J. Jones, C. Y. Cheung, S. Yue and V. L. Singer, *Anal. Biochem.*, 1999, **268**, 278-288.
4. T. Lemarteleur, D. Gomez, R. Paterski, E. Mandine, P. Mailliet and J. F. Riou, *Biochem. Bioph. Res. Co.*, 2004, **323**, 802-808.
5. W. Liu, C. Lin, G. Wu, J. Dai, T. C. Chang and D. Yang, *Nucleic Acids Res.*, 2019, **47**, 11931-11942.
6. S. Forli, R. Huey, M. E. Pique, M. F. Sanner, D. S. Goodsell and A. J. Olson, *Nat. Protoc.*, 2016, **11**, 905-919.